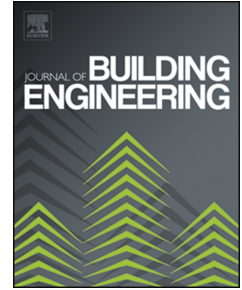# Journal Pre-proof

Near-surface mounted-FRP flexural retrofitting of concrete members using nanomaterial-modified epoxy adhesives

Mohammad Al-Zu'bi, Mizi Fan, Lorna Anguilano

Please cite this article as: M. Al-Zu'bi, M. Fan, L. Anguilano, Near-surface mounted-FRP flexural retrofitting of concrete members using nanomaterial-modified epoxy adhesives, *Journal of Building Engineering* (2024), doi: https://doi.org/10.1016/j.jobe.2024.108549.

This is a PDF file of an article that has undergone enhancements after acceptance, such as the addition of a cover page and metadata, and formatting for readability, but it is not yet the definitive version of record. This version will undergo additional copyediting, typesetting and review before it is published in its final form, but we are providing this version to give early visibility of the article. Please note that, during the production process, errors may be discovered which could affect the content, and all legal disclaimers that apply to the journal pertain.

Near-surface mounted-FRP flexural retrofitting of concrete members using nanomaterial-modified epoxy adhesives

Mohammad Al-Zu'bi [a], Mizi Fan [a*] and Lorna Anguilano [b]

[a] Department of Civil and Environmental Engineering, College of Engineering, Design and Physical Sciences, Brunel University London, United Kingdom, UB8 3PH.

[b] Experimental Techniques Centre, College of Engineering, Design and Physical Sciences, Brunel University London, United Kingdom, UB8 3PH.

Abstract

This study investigates the effectiveness of nanomaterial-modified epoxy adhesives (NMEAs) for NSM-FRP flexural retrofitting of concrete. A total of 48 specimens (i.e. prisms) were retrofitted using three different types of FRP reinforcement bars (CFRP, GFRP, and BFRP) inserted in grooves with sizes of 8×8, 10×10 or 12×12 mm and bonded to the concrete substrate using either neat epoxy (NE) or NMEAs. NMEAs were developed by incorporating either carbon-based (i.e. CNF, cellulose, and graphite) or silicon-based (i.e. silica and MMT clay) nanoparticles into epoxy at 0.1 wt.% while the graphite NMEAs were prepared with more wt.% (i.e. 0.2 and 0.3). SEM and XRD techniques were used to assess the dispersion quality of nanoparticles within the matrix, along with the % porosity and % crystallinity of the NMEAs. Results showed that using silica, clay, and graphite NMEAs rather than NE enhanced the retrofitted concrete capacities, whereas a strength decrease was observed when using CNF- and cellulose-modified epoxies. Moreover, it was found that the specimens bonded with silicon-based NMEAs had, on average, higher capacities than those bonded using carbon-based NMEAs, which, on the other hand, showed more ductile behaviour. The results also suggested that the capacities of the specimens decreased with increasing the wt. % concentration of the nanoparticles (i.e. graphite). Increasing the groove size from 8×8 mm to 10×10 mm decreased the capacities but enhanced the ductility, whereas increases in both the capacities and ductility were achieved when moving from 8×8 mm to 12×12 mm.

1. Introduction

The effectiveness of retrofitting concrete members with fibre reinforced polymer (FRP) materials has been found to highly depend on the type of the bonding agent (i.e. the adhesive) used to bond the FRP reinforcement to the concrete substrate, because the adhesive layer, indeed, works as a medium to transfer and distribute stresses between concrete and FRP materials. Therefore, the properties of adhesives play a key role in enhancing the bond characteristic and strength of the FRP-adhesive-concrete interfaces, and attention must be paid to selecting suitable bonding agents for successful retrofitting processes [1-3].

Using neat epoxy (NE) adhesives in concrete retrofitting in both Externally Bonded Reinforcement (EBR) and Near Surface Mounted (NSM) retrofitting systems has been found effective in bonding FRP composites to the substrate of existing concrete members to improve their strength, stiffness and integrity [2-6, 37]. Nevertheless, the retrofitting of concrete members using FRP composites has some drawbacks regarding the performance of the epoxy layer, including the debonding of the FRP materials from the concrete substrate, which may be caused by the non-uniform stress distribution between concrete-adhesive and FRP-adhesive interfaces, and eventually resulting in premature debonding failure of the FRP-retrofitted concrete members [7-10]. Furthermore, the highly cross-linked epoxy resins are rigid and brittle, and have relatively poor resistance to crack initiation and growth, which limit their use in structural retrofitting [5, 10], since such issues would negatively affect the structures' durability and are also unacceptable from the structural safety perspective. Hence, there is an urgent need to enhance the performance of epoxies so they can be used effectively in retrofitting applications.

Owing to their extraordinary thermo-mechanical properties, incorporating nanoparticles into epoxy adhesives has been found able to overcome the drawbacks associated with using NE adhesives in the EBR-retrofitted members through enhancing their mechanical properties and interfacial bond between FRP reinforcement and concrete substrate [1, 2, 11-15]. For instance, Irshidat et al. [1] studied the effect of using both NE and epoxy modified with carbon nanotubes (CNTs) on the flexural capacities of reinforced concrete (RC) beams strengthened by carbon FRP (CFRP) sheets. The results suggested that using CNTs-modified epoxy slightly increased the ultimate loads of the beams by about 5% and significantly enhanced their stiffness and toughness by about 35% and 28%, respectively. It was also found that using modified adhesive could delay the propagation and debonding of CFRP sheets, which was attributed to the enhancement of the concrete-epoxy adhesion. In a further study [2], the influence of CNTs-modified epoxy on the

bond-slip behaviour between concrete surface and carbon and glass FRP sheets in concrete prisms was investigated. The results showed that using CNTs-modified epoxy resin enhanced the bond strength and slip at failure of the tested specimens by 35% and 52% in the case of carbon fibre and by 26% and 83% in the case of glass fibre, respectively. Moreover, the NE-bonded specimens failed due to debonding at the interface between fibre sheet and concrete surface, while a cohesive failure occurred in the specimens bonded using CNTs-modified epoxy. Another study [12] on strengthening RC columns with CNTs-modified epoxy exhibited that the axial load-carrying capacity and toughness of wrapped columns increased by 12% and 19%, respectively with using CNTs-modified epoxy over those bonded using NE. However, both CNT's and NE specimens showed a ductile failure mode. The use of multi-walled CNTs (MWCNTs) in repairing and strengthening epoxy resin systems for FRP-confined concrete cylinders was investigated by Rousakis et al. [15]. The results confirmed the potential of the MWCNTs-reinforced epoxy resins for use in advanced crack repair of high-performance concrete.

It has also been confirmed that incorporating other carbon-based nanomaterials, such as CNFs [38-42], graphene and graphite [43-49] and cellulose nanocrystals (CNCs) [50-55] into epoxy resins could enhance their mechanical properties and were also found to provide outstanding reinforcing potential and demonstrates efficient stress transfer behaviour. In addition, silicon-based nanomaterials, such as silica [56-59] and clay [60, 61] nanoparticles, have also showed their efficiency in improving the mechanical performance of epoxy polymers. However, there is currently no evidence of applying these epoxy nanocomposites in the NSM-FRP structural retrofitting of concrete members.

It was also observed that the behaviour of the flexural-retrofitted and -strengthened concrete members are also affected by other parameters, such as type of FRP reinforcement [24, 25] and the groove size/dimensions [26-28]; Abdallah et al. [24] found that using NSM-GFRP bars could lead to about 24% ductility improvement compared to using CFRP bars, while the load-carrying capacity of the NSM-GFRP-strengthened beams was about 77% of those strengthened with CFRP bars, which also achieved higher stiffness. Another investigation [25] found that the yield and ultimate loads of the CFRP-reinforced beams were also found consistently higher than GFRP counterparts by 23% and 19.7%, respectively. However, the mid-span ultimate displacement and ductility factor dropped by 45% and 69%, respectively, which resulted in higher steel strains, indicating lower utilization ratio of the FRP reinforcement. For the groove size effect, using smaller groove width (e.g. 1.5*strip width (b_b) rather than 2.0b_b) was found to achieve higher load

capacity (28%), ductility (44%) and energy absorption (84%), and also delayed the debonding failure [27]. Additionally, it was reported that the resistance to concrete split failure increases with the groove width [28].

It could be concluded from previous that the application of nanomaterial-modified epoxy adhesives (NMEAs) for structural retrofitting has been addressed by only few research studies. In addition, the research work done so far is still limited to the EBR-FRP strengthening/retrofitting applications and only focused on using the CNTs as adhesive Nano-fillers. Thus, investigating the effect of using NMEAs in the NSM-FRP applications is highly required to explore the full potential of NMEAs for high-performance retrofitting and bonding systems, and to obtain in-depth understanding of the reactivity of bonding agents and FRP reinforcements and their correlations. Besides, more investigation on the behaviour of the NSM-FRP-retrofitted concrete members with different FRP reinforcement types and groove dimensions is required in order to establish a correlation between retrofitting parameters and structural performance for optimum retrofitting design.

The present study intends to fill those research gaps with a comprehensive laboratory investigation focused on the use of the NMEAs in the NSM-FRP applications. To this scope, a series of concrete prisms (50 x 50 x 200 mm^3) were retrofitted and tested under 3-point bending with the purpose of evaluating the influence of various parameters on the effectiveness of NMEAs-bonded novel NSM-FRP flexural retrofitting, including (I) type of FRP reinforcement, (II) type of bonding agent, (III) type of nanoparticles in the NMEAs, (IV) wt.% of nanoparticles into epoxy and (V) groove size. The results are presented and analysed in terms of the structural behaviour (i.e. ultimate capacity and ductility) of the tested specimens in addition to the observed failure modes. Additionally, the microstructure, in terms of the dispersion of the nanoparticles across the matrix and the % porosity of the NE and the nanocomposites, in addition to their % crystallinity were investigated by means of Scanning Electron Microscopy (SEM) and X-ray Diffraction (XRD) analyses, respectively to further deepen the understanding of the performance of the NMEAs for their application as bonding agents in the NSM-FRP retrofitting applications. It's noteworthy that the terms NMEAs and nanocomposites are used interchangeably through the paper.

2. Experimental programme

2.1 Material properties

1. Concrete

Concrete with 28-day average compressive strength of 29.6 MPa, determined on standard concrete cylinders (i.e. 100 mm diameter x 200 mm height), was prepared. Concrete mix design is listed in Table 1.

2. FRP reinforcement

CFRP, GFRP and BFRP round bars with 6 mm diameter were used for the purpose of this study (Fig. 1). Their mechanical properties are shown in Table 2. The CFRP bars were provided by Sika Limited, UK, while Engineered Composites Ltd, UK provided the GFRP and the BFRP bars.

The versatility of CFRP, the resilience of GFRP, and the eco-friendly nature of BFRP make them compelling choices for enhancing structural integrity. Capitalizing on the NSM technique's strong bond with these distinct FRP materials presents a robust solution for reinforcing concrete elements. By integrating CFRP's exceptional strength-to-weight ratio, GFRP's corrosion resistance, and BFRP's inherent durability, this retrofitting strategy promises to effectively enhance load-bearing capacity, deter crack propagation, and extend the lifecycle of the structure. This integrated approach marries the unique attributes of CFRP, GFRP, and BFRP with the efficacy of NSM retrofitting, resulting in a comprehensive and sustainable solution for enhancing the performance and longevity of concrete members

3. Epoxy adhesive

Sikadur®-30, a thixotropic, structural 2-component adhesive, based on a combination of epoxy resin and hardener (i.e. A & B) was used. Its properties are shown in Table 2. Epoxy was provided by Sika Limited, UK.

4. Nanomaterials

Five different nanoparticles, which are: carbon nanofibres (CNF), silica Nano powder, cellulose nanocrystals (CNCs), MMT Nano clay and graphite Nano powder, were used for the purpose of this study. Their composition and properties are listed in Table 3.3. The nanomaterials were provided by Nanografi, Turkey. Their description and properties are listed in Table 3.
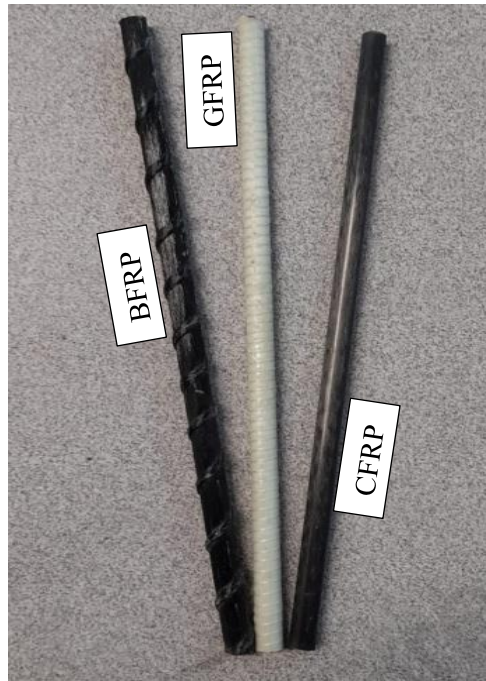
Fig. 1. FRP reinforcement bars used in this study.

Table 1. Concrete mix design.

C: S: Agg. = 1:1:2 (by volume)			
Ingredient	**Description**	**Density (Kg/m^3)**	**Quantity (Kg/m^3)** (w/c = 0.50)
Cement (C)	Type I Ordinary Portland cement (OPC)	1360	340
Coarse aggregate (Agg.)	Crushed stones with angular edges (1mm < size < 5mm)	1560	780
Sand (S)	Sharp silica sand with uniform grain size (250μm < size < 1mm)	1590	397.5
Water	Tap water	1000	170

Table 2. Mechanical properties of the FRP bars and epoxy adhesive (As per suppliers).

Material \ Property	Tensile strength (MPa)	E-modulus (GPa)	Elongation at break (%)
CFRP (Sika® CarboDur® BC 6)	3100	148	1.6
GFRP	1280	> 40	N/A
BFRP	1000	≥ 45	N/A
Epoxy adhesive	29	11.2	N/A

6

Table 3. Description and physical properties of nanomaterials (As per supplier).

Nanomaterial description (Purity)	Particle size	Density (g/cm³)	Specific Surface Area (SSA) (m²/g)
Carbon Nanofibers (CNF) (> 96%)	Outside Diameter: 190-590 nm, Length: 5.0-55.0 µm	2.2	20
Silicon Dioxide (SiO₂) Nano powder/Nanoparticles, coated with 2 wt.% Silane (97.3+ %)	16 nm (average)	2.2	150-550
Cellulose Nanocrystals (Nanocrystalline Cellulose, CNC) (92 %)	Width: 10-20 nm, Length: 300-900 nm	1.49	~ 14
montmorillonite (MMT) Nano clay (99.9 %)	800 nm	2.35 (Avg.)	Up to 450
Graphite (C) Nano powder/Nanoparticles (99.9 %)	< 50 nm	2.26	> 100

2.2 Specimen preparation and test setup

2.2.1 Preparation of the NE and the NMEAs

NE adhesive was prepared by manually mixing the two components: part A (resin) and part B (hardener) (A: B = 3:1 by weight as recommended by the manufacturer) for 4 min. For the NMEAs, some drops of acetone were first added to the nanoparticles and manually stirred for 3 min to improve their dispersibility and to reduce agglomeration. Afterwards, the epoxy part A was carefully weighed and manually mixed for 2 min in a suitable beaker with the pre-weighted nanoparticles. The mix was then carried out through a high-intensity ultrasonic irradiation for 5 min. Once the irradiation was completed, part B was added to the modified part A and manually mixed for 2 min. The samples were then left for 7 days at room temperature to cure. A schematic of the synthesis of the NMEAs is illustrated in Fig. 2.

The SEM analysis was meticulously conducted using two distinct microscopes: The Zeiss LEO and the Zeiss Supra 35VP, both equipped with high field emission capabilities designed to capture intricate micro images of the tested samples. The selection of the imaging mode was a strategic decision influenced by the unique characteristics of each sample and the specific capabilities offered by each microscope. In particular, the Zeiss LEO microscope was purposefully chosen for the analysis of the NE and the clay nanocomposites. This selection was based on its proven suitability for generating high-quality micro images of these specific samples, ensuring a detailed and accurate representation. Conversely, the Zeiss Supra 35VP

7

microscope, renowned for its superior magnification capabilities, was exclusively employed for analysing the remaining samples. This deliberate choice aimed to guarantee optimal imaging outcomes, especially for nanocomposites prepared with smaller nanoparticles, where the use of higher magnification becomes imperative to capture and depict finer details with precision. Moreover, the SEM images of samples' surfaces were also analysed through ImageJ software for the porosity study.

The XRD analysis was carried out using a Bruker D8 Advance diffractometer equipped with copper tube and Lynxeye position sensitive detector, and then the crystallinity of each sample was obtained from Eva software based on the diffractogram.
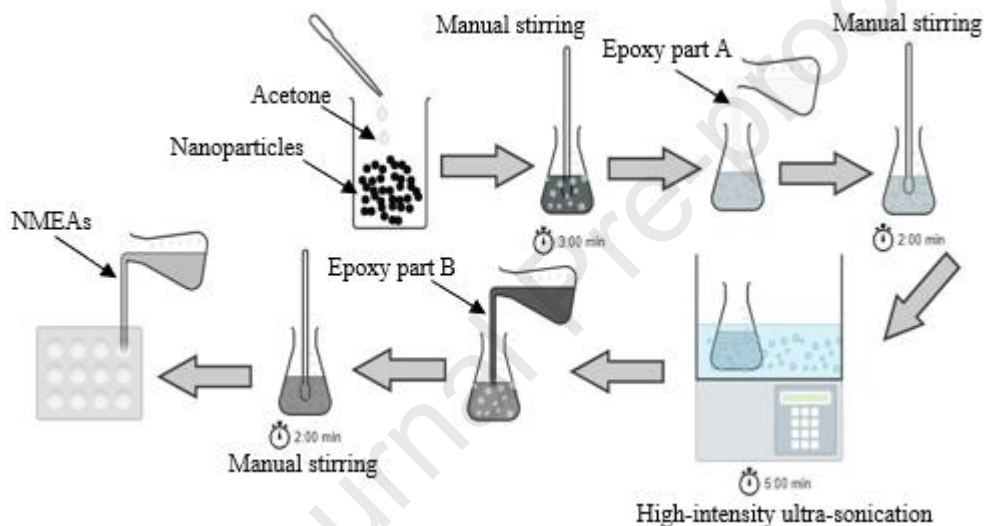

Fig. 2. Synthesis of the NMEAs.

First, the adoption of a straightforward, simple and cost-effective mixing method in the preparation of the nanocomposites was a deliberate choice made with the aim of optimizing efficiency without compromising quality. While more complex and resource-intensive techniques exist, this approach has demonstrated its effectiveness in achieving homogeneity and ensuring relatively uniform distribution of nanoparticles within the epoxy matrix (as shown in the results). Furthermore, its simplicity allows for easy scalability and reproducibility, making it a practical choice for research and industrial applications.

Furthermore, the epoxy adhesive was cured for 7 days before use for characterization (also for retrofitting purposes) purposes to ensure maximum strength and durability. This extended curing period allows the epoxy to reach its full chemical and mechanical properties (as per supplier), providing reliable and consistent performance in various applications. It ensures that

the adhesive is fully bonded and hardened, enhancing its load-bearing capacity, chemical resistance, and long-term stability, making it a dependable choice for demanding projects.

2.2.2 NSM-FRP retrofitting of concrete specimens

For the purpose of NSM-FRP retrofitting of concrete specimens, a total of 16 prisms (Fig. 3), three replicates each, with dimensions of 50 x 50 x 200 mm^3 were cast and retrofitted with 6 mm diameter CFRP, glass FRP (GFRP) or basalt FRP (BFRP) bonded using either NE or NMEAs. The following test parameters were considered for the purpose of this study:

- type of FRP reinforcement: the effect of using three different types of FRP reinforcement bars, that is, CFRP, GFRP and BFRP bars, was investigated;
- type of bonding agent: two different bonding agents, namely NE and NMEAs, were considered to bond the FRP reinforcement bars;
- type of the nanoparticles: two groups of nanomaterials were incorporated into epoxy at 0.1 wt.%, which are (1) carbon-based nanomaterials including CNF, CNCs and graphite nanoparticles, and (2) silicon-based nanomaterials comprehending silica nanoparticles and montmorillonite (MMT) Nano clay;
- wt.% concentration of the nanoparticles: this parameter was only considered in the graphite NMEAs, where two more wt.% concentrations, e.g. 0.2 and 0.3 wt.% were utilised; and
- groove size: the effect of three groove dimensions (width x depth), that is, 8x8, 10x10 and 12x12 mm giving 1.33, 1.67 and 2.00 ratio of groove width or depth to FRP bar diameter (b/d$_b$), was investigated in the specimens bonded with NE or graphite NMEAs.

The retrofitting design of tested specimens is provided in Table 4. The specimens bonded with the NMEAs were designated in the form of W-X-Y-Z as follows: W indicates the FRP type (i.e. C for CFRP, G for GFRP and B for BFRP), while X indicates the type of the bonding agent (i.e. S for silica, Cl for clay and Gr for graphite NMEAs). Y is the wt.% concentration of the nanomaterials (i.e. 0.1, 0.2 or 0.3) and Z indicates the groove size (i.e. 8, 10 or 12). For example, the specimen C-Gr-0.1-8 is that retrofitted with CFRP bar inserted in an 8x8 mm groove and bonded using graphite NMEAs prepared at 0.1 wt.% concentration.

Table 4. NSM-FRP retrofitting design.

Specimen	Bonding agent	Nanoparticles (NP)	NP wt.% concentration	FRP reinforcement bars	Groove dimensions (width x depth) [mm²]
C-NE-8	NE	-	-	CFRP	8 x 8
G-NE-8		-	-	GFRP	
B-NE-8		-	-	BFRP	
C-CNF-0.1-8	NMEAs	CNF	0.1	CFRP	8 x 8
C-S-0.1-8		Silica			
C-CNC-0.1-8		CNCs			
C-Cl-0.1-8		Clay			
C-Gr-0.1-8	NMEAs	Graphite	0.1	CFRP	8 x 8
G-Gr-0.1-8				GFRP	
B-Gr-0.1-8				BFRP	
C-NE-10	NE	-	-	CFRP	10 x 10
C-Gr-0.1-10	NMEAs	Graphite	0.1	CFRP	10 x 10
C-NE-12	NE	-	-	CFRP	12 x 12
C-Gr-0.1-12	NMEAs	Graphite	0.1	CFRP	12 x 12
C-Gr-0.2-12			0.2		
C-Gr-0.3-12			0.3		

Fig. 3. Concrete prisms to be retrofitted.

The NSM-FRP retrofitting process was implemented on the concrete specimens starting with the roughening of the groove sides using sandpaper. The grooves were subsequently cleaned using an air compressor to eliminate any generated dust. Following this, the grooves were partially filled with adhesive, employing a trowel. Afterwards, the FRP reinforcement bars were positioned within the grooves and gently pressed, enabling the paste to flow around the bar and to fully fill the space between the bars and the groove sides. Finally, the grooves were filled with additional adhesive, and the surface was levelled.

The retrofitted specimens were then air-cured at room temperature for 7 days to guarantee a proper curing of the adhesive and to ensure sufficient bond between concrete, adhesive and FRP reinforcement, and to simulate the curing time and conditions of the NE and the NMEAs samples (section 2.2.1). Retrofitting process is shown in Fig. 4.

The three-point bending test was conducted using an INSTRON 5969 Universal testing machine under a 150 kN load cell with a crosshead speed of 1.04 MPa/min (avg.) according to the ASTM C 78-02 [20]. The ultimate loads, flexural strength and displacements at maximum loads (described as maximum displacements through the paper) were then recorded using a data acquisition system, and the accompanying modes of failure were also monitored.
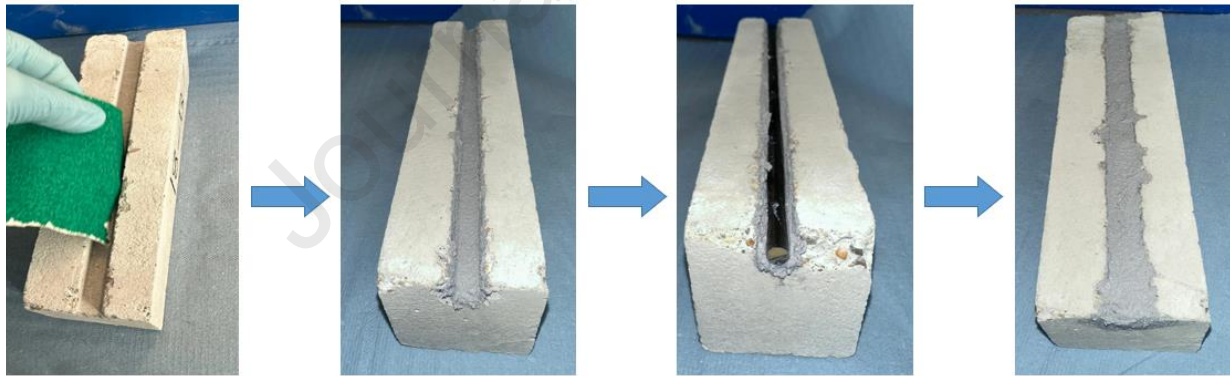

Fig. 4. NSM-FRP retrofitting of concrete specimens.

3. Results and discussion
3.1 Characterisation of the NE and the NMEAs samples
3.1.1 SEM and porosity analyses

The NMEAs samples were analysed through SEM (Fig. 5a) to investigate their microstructure, morphology in addition to the degree of dispersibility of the nanoparticles through the matrix. The % porosity analysis was also conducted on the SEM images of the samples' surfaces (Fig. 5b) and the results are provided in Table 5.

11
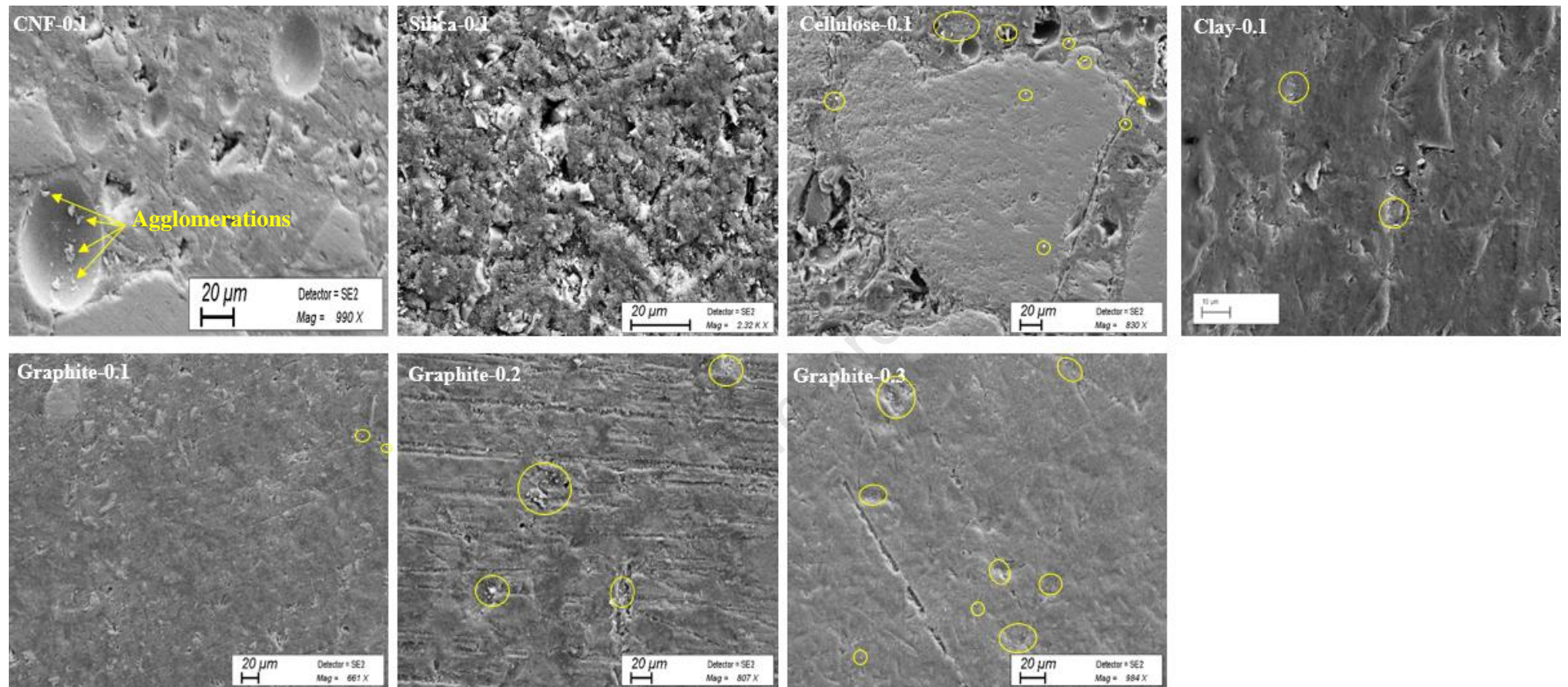
(a)
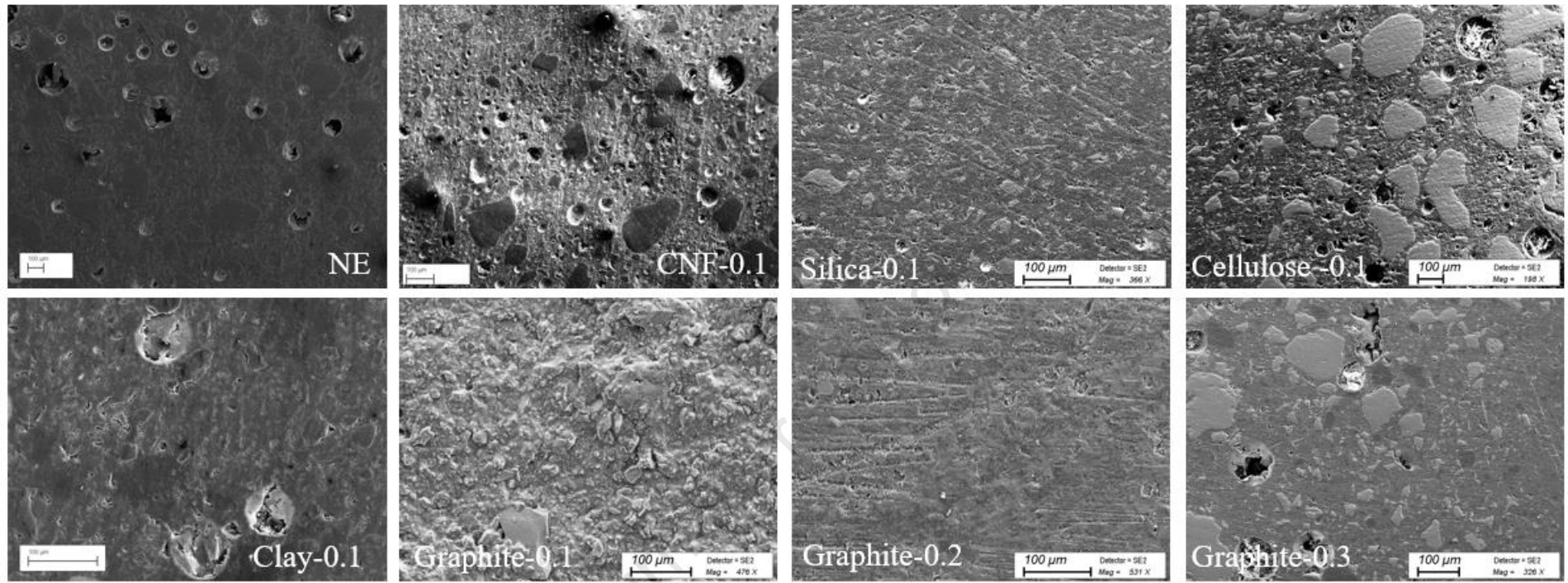
(b)

Fig. 5. SEM images of (a) the NE and the NMEAs samples and (b) their surfaces.

As shown in Fig. 5a, the CNF nanocomposite had particles agglomerating within the matrix, while it could be seen that the silica nanoparticles are uniformly-dispersed through the adhesive. Whereas many particles aggregating are shown in the cellulose sample. An insignificant amount of clay particles clustering through the matrix. The graphite-0.1 sample was noticed to have very few agglomerations, which seem to increase with the wt.%.

Table 5. % Porosity of the NE and the NMEAs.

Sample	% Porosity	% Porosity increase (+) or decrease (-) compared to the NE
NE	2.015	-
CNF-0.1	2.407	19.5
Silica-0.1	1.727	-14.3
Cellulose-0.1	2.704	34.2
Clay-0.1	1.814	-10.0
Graphite-0.1	1.386	-31.2
Graphite-0.2	1.492	-26.0
Graphite-0.3	2.228	10.6

For the % porosity, the NE sample has significant amount of air voids showing up on its surface. For the NEMAs, it was observed that the nanoparticles that dispersed well within the matrix could fill the gaps between polymer chains, leading to a more compact structure with fewer voids. In addition to that, those uniformly-dispersed nanoparticles act as nucleation sites for polymer crystallization (discussed in detail in section 3.1.2), promoting the formation of ordered structures and reducing the occurrence of voids during the curing process.

The presence of the well-dispersed nanoparticles can also enhance the packing efficiency of the epoxy matrix, due to their small size and high surface area, nanoparticles can fit more closely together, reducing the interstitial spaces and minimizing porosity. Moreover, some nanoparticles have barrier properties that can hinder the diffusion of gases (i.e. air bubbles) through the matrix. This property can prevent the incorporation of air voids or pockets, contributing to a lower overall porosity. Furthermore, the nanoparticles that have exceptional mechanical properties can reinforce the epoxy matrix and hinder the propagation of micro cracks, consequently reducing porosity associated with crack formation.

On the other hand, it was also observed that the modified nanocomposites could have an increased porosity over than that of the NE, which could be due to that the agglomeration of nanoparticles within the matrix, which would lead to the formation of nanoparticle clusters. These clusters can create localized regions of high viscosity, making it difficult for the epoxy to flow and fill all the void spaces effectively during curing. As a result, trapped air may be

14

incorporated into the composite, leading to increased porosity. Moreover, uneven dispersion can hinder the nanoparticles from effectively filling the interstitial spaces, creating voids and ultimately increasing porosity. Additionally, the incorporation of nanoparticles can alter the curing kinetics of the epoxy matrix, as they may affect the curing process, leading to incomplete curing and the presence of unreacted or partially reacted epoxy, resulting in increased porosity. Also, the porosity increases as the curing time decreases, which is because of that there would be no enough time for the air bubbles to come out of the samples. So, the faster the curing the higher the porosity.

3.1.2 Crystallinity analysis

The % crystallinity of the NE and the NMEAs samples are provided in Table 6. The analysis results showed that adding 0.1 wt.% CNF and cellulose to epoxy decreased its crystallinity by about 5 % and 14%, respectively. For the CNF nanocomposites, the crystallinity reduction could be due to that the presence of CNF would create a physical barrier hindering the mobility of epoxy chains and reduce their ability to form ordered structures. As a result, the polymer chains are less able to freely move and align themselves in a regular pattern, which is necessary for the formation of crystalline regions. Moreover, since crystallization requires the presence of nucleation sites where crystal growth can initiate, the introduction of CNF, in some cases, can disrupt these sites or prevent their formation, leading to a reduced crystallinity. For the cellulose-epoxy nanocomposites, the reduction of crystallinity was ascribed to the strong interaction of the cellulose with the OH groups of the epoxy forming a twisted mass, causing steric effect, which resulted in the destruction of the epoxy-ordered structure, as confirmed in the literature [33, 62]. It was also observed that incorporating 0.3 wt.% graphite nanoparticles led to approximately 6% reduction in the crystallinity of the NE, which was ascribed to that, as confirmed in [34], the exfoliated state of graphite, which restricted the free movement of polymer chains to arrange themselves in an orderly fashion, hindering the crystallization and therefore reducing its crystallinity. Moreover, in the case of adding a high concentration of the graphite nanoparticles to the epoxy, the particles act as fillers and could dilute the concentration of the polymer chains. This dilution effect reduces the ability of the epoxy chains to organise and crystallize, leading to a decrease in overall crystallinity of the producing composite.

On the other hand, the epoxy samples filled with 0.1 wt.% silica, clay and graphite (and 0.2 wt.%) nanoparticles yielded about 19%, 6%, 18% and 7% crystallinity increase, respectively. For the silica nanocomposites, the presence of the silica nanoparticles can enhance the mobility of the epoxy chains during curing and solidification. The improved chain mobility would allow

the polymer chains to rearrange more effectively and form well-organized crystalline structures. Moreover, the strong interfacial interactions between the silica nanoparticles and the epoxy matrix can lead to better alignment and arrangement of the chains, contributing to increased crystallinity. The clay nanoparticles can act as templates for the organization of epoxy chains. In addition, the layered structure of clay provides a favourable environment for the alignment and arrangement of polymer chains, leading to the formation of crystalline regions, and eventually increasing the crystallinity. Graphite nanoparticles can hinder the mobility of epoxy chains during curing and solidification. The hindered chain mobility can restrict the movement of the chains, facilitating the formation of crystalline regions. Furthermore, the enhanced interfacial interactions between graphite nanoparticles and the epoxy matrix have the potential to facilitate improved chain alignment, thereby promoting the process of crystallization, since the interaction between the nanoparticles and the matrix could influence the conformation and packing of polymer chains.

It's worthy to note that the crystallinity of epoxy can have a significant impact on its mechanical properties and the interfacial bonding characteristic with the matrix material [36]. For instance, since the crystalline regions act as reinforcing elements within the epoxy matrix, the increased crystallinity would provide additional resistance to deformation and enhance the overall strength and stiffness of the material. On the other hand, the less crystalline epoxies are generally more ductile and less prone to brittle fracture compared to the crystalline ones, which may be more rigid and susceptible to brittle failure. These are reflected in the retrofitted results which are discussed in next sections.

Table 6. % Crystallinity of the NE and the NMEAs.

Sample	% Crystallinity	% Crystallinity increase or decrease compared to the NE
NE	65	-
CNF-0.1	61.5	-5.4
Silica-0.1	77.6	19.4
Cellulose-0.1	56.2	-13.5
Clay-0.1	68.7	5.7
Graphite-0.1	76.5	17.7
Graphite-0.2	69.4	6.8
Graphite-0.3	61.2	-5.8

3.2 Behaviour of retrofitted prisms subjected to bending load

A total of 48 three-point bending tests were conducted for the purpose of this study. It's noteworthy that, as mentioned previously, three replicates (i.e. A, B and C) of each configuration

were prepared and the average capacities (i.e. ultimate loads, max flexural strength and the maximum displacement (i.e. ductility)) were obtained and are summarised in Table 7. The failure mode of each replicate was addressed individually. The effect of the different parameters on the overall flexural capacities, ductility and the failure modes of the tested specimens are discussed in the following sections.

Table 7. Overall capacities and failure modes of tested specimens.

Specimen	Avg. ultimate load (kN) (COV*)	Avg. max flexural strength (MPa)	Avg. max displacement (mm) (COV)	Failure mode
C-NE-8	14.75 (0.04)	26.55	1.27 (0.09)	Shear and debonding
G-NE-8	14.86 (0.07)	26.75	1.84 (0.12)	Flexural
B-NE-8	14.85 (0.19)	26.73	2.02 (0.05)	Shear and flexural
C-CNF-0.1-8	9.33 (0.13)	16.79	1.89 (0.22)	Shear and flexural
C-S-0.1-8	17.22 (0.09)	30.99	1.57 (0.08)	Shear and debonding
C-CNC-0.1-8	13.36 (0.15)	24.05	1.73 (0.05)	Shear
C-Cl-0.1-8	15.45 (0.08)	27.81	1.51 (0.28)	Shear and debonding
C-Gr-0.1-8	16.92 (0.08)	30.45	1.12 (0.14)	Shear and flexural
G-Gr-0.1-8	15.39 (0.12)	27.70	1.85 (0.09)	Shear and flexural
B-Gr-0.1-8	15.20 (17)	27.36	1.99 (0.18)	Flexural and concrete crushing
C-NE-10	21.67 (0.16)	38.99	1.61 (0.11)	Shear
C-Gr-0.1-10	16.05 (0.15)	28.89	1.82 (0.20)	Shear
C-NE-12	12.98 (0.13)	23.37	1.84 (0.12)	Shear and concrete crushing
C-Gr-0.1-12	19.06 (0.17)	34.31	1.31 (0.30)	Shear and concrete crushing
C-Gr-0.2-12	18.43 (0.12)	33.18	1.48 (0.12)	Shear
C-Gr-0.3-12	12.19 (0.12)	21.95	1.59 (0.27)	Shear and concrete crushing

*Coefficient of variation

3.2.1 The effect of the FRP reinforcement type
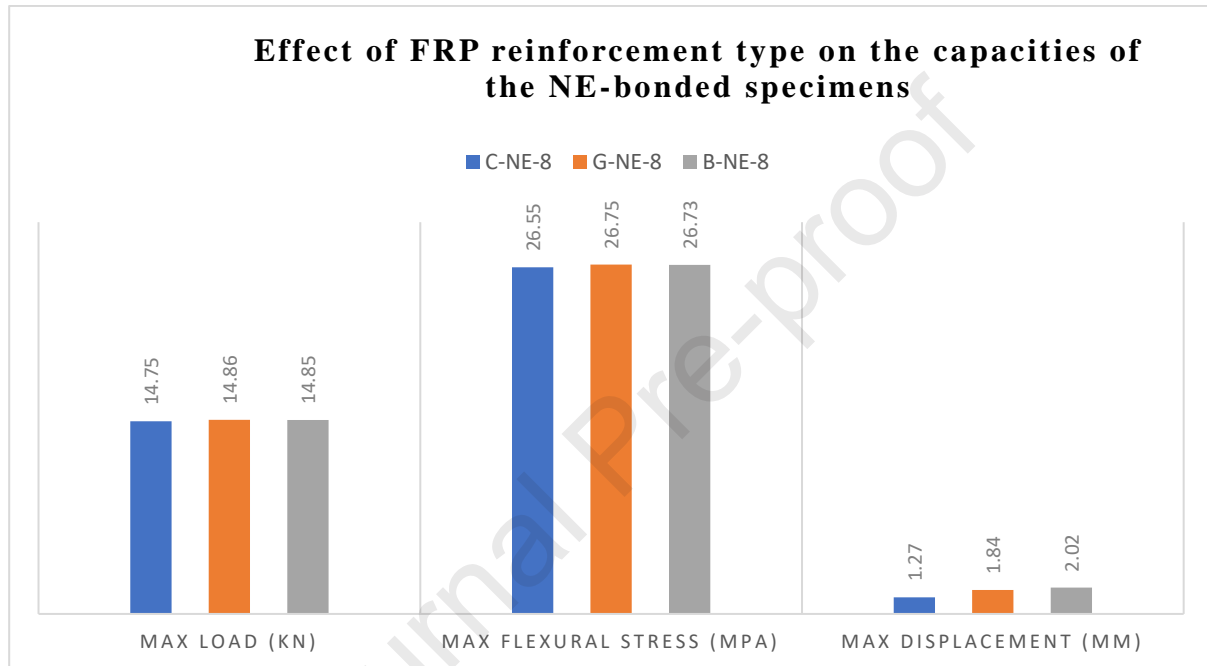
Overall flexural capacities and ductility response

The effect of retrofitting specimens with CFRP, GFRP and BFRP bars on their flexural behaviour is discussed in this section. It's noteworthy that two groups of specimens are considered herein. The first group includes the NE-bonded specimens (i.e. C-NE-8, G-NE-8 and B-NE-8), while the NMEAs-bonded specimens (i.e. C-Gr-0.1-8, G-Gr-0.1-8 and B-Gr-0.1-8) are considered in the second group.

For the specimens bonded with NE, the capacities in terms of maximum load or flexural strength, of the GFRP- and the BFRP-retrofitted specimens were very close, which were only 1% higher than those retrofitted using CFRP bars. This observation agrees with what was found by Soliman et al. [16]. The ductility was found to be the highest in the case of the BFRP-retrofitted specimens, which showed about 59% and 10% higher maximum displacement than those retrofitted by CFRP and GFRP rods, respectively. While using GFRP reinforcement bars, exhibited about 45% increase in the ductility than those retrofitted with CFRP bars. This could be, as confirmed in the literature [16, 17], due to that the mechanical properties (i.e. tensile strength and elastic modulus), as shown in Table 3, of the CFRP bars are much higher than those of the GFRP bars, which in turn has higher mechanical properties than those of the BFRP bars.

On the other hand, changing the type of the FRP reinforcement in the specimens bonded with the graphite-modified epoxies was found to have more influence on the bending behaviour in terms of load-carrying capacity and ductility. For instance, using CFRP bars showed about 10% and 12% flexural capacity increase, respectively compared to utilising GFRP and BFRP bars, which could be due to the high mechanical properties of the CFRP rods compared to those of the other FRP's. While a slight increase in the capacity was reported when using the GFRP bars rather than the BFRP ones. Regarding the ductility, about 44% and 8% higher maximum displacement were reported in the case of utilising BFRP bars, respectively, than when CFRP and GFRP rods were used, which could be due to the same reason mentioned above, which would justify the 65% higher ductility that was exhibited in the GFRP-retrofitted specimens over those retrofitted by CFRP bars.

Consequently, the performance in terms of the load-carrying capacity was pretty much similar in the case of bonding specimens with NE, so it was difficult to determine the most efficient FRP bars to be used, while using the modified adhesive revealed the best FRP choice more clearly.

18

Furthermore, similar observations to those found in the NE-bonded specimens in regard with the maximum displacement were reported using the modified adhesive. However, the % increase were a bit different. Where compared to using the NE adhesive, using modified adhesive lowered the % increase in the ductility from 59% to 44% and from 10% to 8% when moving from BFRP reinforcement to GFRP and to CFRP, respectively. In contrast to that, a higher % increase (i.e. from 45% to 65%) was observed when moving from GFRP to CFRP. A graphical representation of the results is depicted in Fig. 6.
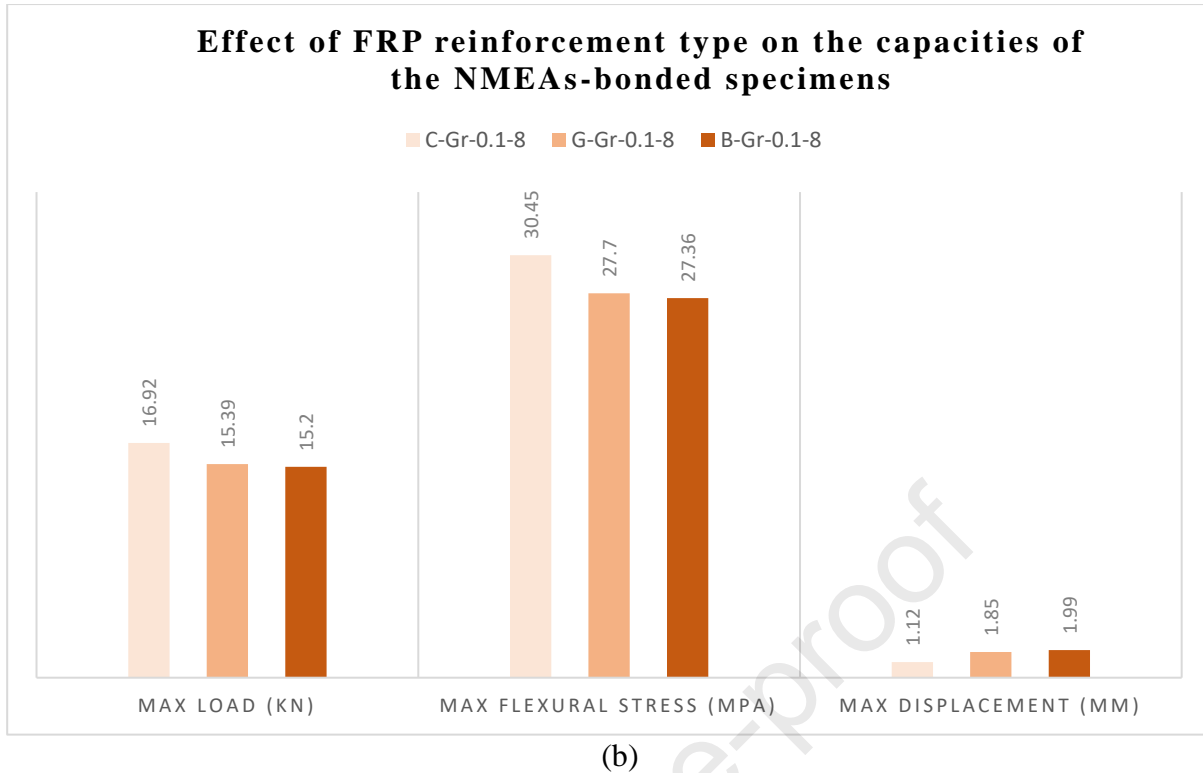

(a)

Effect of FRP reinforcement type on the capacities of the NMEAs-bonded specimens

■ C-Gr-0.1-8　■ G-Gr-0.1-8　■ B-Gr-0.1-8

(b)

Fig. 6. Effect of FRP type on the capacities of (a) the NE-bonded specimens and (b) the NMEAs-bonded specimens.

Failure modes

The failure modes of the specimens retrofitted with different FRP reinforcement types are shown in Fig. 7. In the first group, which includes the NE-bonded specimens, specimens C-NE-8 (i.e. A, B and C), which were retrofitted by CFRP bars, mainly failed in shear. Where in specimen A, as shown in Fig. 7a (on the left), the shear crack generated in concrete and continued to pass through the epoxy layer but with less width than in the concrete, since epoxy is stronger, which was able to stop its progress. Similar mode of failure was noticed in specimen C (on the right), but the crack continued to progress through concrete after it passed the epoxy layer, which was able to curb the crack to pass through it in specimen B (in the middle), but that led to debonding (i.e. CFRP bar slippage) at the FRP-epoxy interface. This could arise because of the smooth surface of the CFRP rods (Fig. 1), which did not provide enough bond strength with epoxy.

Unlike what was observed in C-NE-8, flexural failure was the dominant in G-NE-8 (Fig. 7b), which were retrofitted with GFRP bars. In specimen A, a wide flexural crack generated into concrete and broke through the epoxy layer to the other side, and also kept progressing align to the GFRP-epoxy interface resulting in a partial peeling-off of the epoxy layer at the bar-epoxy interface and causing a part of concrete to detach. Specimen B failed by approximately the same

20

manner, but the epoxy layer did not peel off. Similar observations were reported in specimen C, but the major crack that led the specimen to fail was narrower than those appeared in the previous specimens.

A combined shear and flexural failure mode were shown in the specimens retrofitted with BFRP bars (i.e. B-NE-8) (Fig. 7c), where main flexural crack alongside minor shear crack, appeared in specimen A, which aligned with the adhesive line at the concrete-epoxy interface leading parts of concrete to peel off with thin layers of epoxy stuck on them. Similar observations were reported in regard with specimen B, with a bit more cracks appeared on concrete surface at failure, however no peeling off took place. Different failure mode was noticed in specimen C, which mainly failed due to number of shear cracks appeared at failure, that did not align with the epoxy line, but alternatively crossed it only in one place, in addition to that the epoxy line was able to limit the crack from progressing to the other side of the specimen. Contrary to what was observed in C-NE-8 and G-NE-8, fewer visible cracks were able to penetrate the epoxy layer, which indicates a stronger bond at the concrete-epoxy-BFRP interfaces.

In the specimens bonded with NMEAs (i.e. group 2), on the other hand, changing the type of the FRP reinforcement led specimens to fail in different ways. For example, CFRP bars that was used in C-Gr-0.1-8 (Fig. 7d) caused a shear failure in specimen A, which was represented by a major shear crack, which began as flexural, appeared in the concrete body with a short tail continued to align with the adhesive line, which was approximately the same that happened in specimen C. Specimen B exhibited a similar failure mode, but the shear crack was less broad, which gave the opportunity to the flexural crack to generate, which had longer tail lying on the edge of the adhesive line, but without breaking through it. Contrary to that, the cracks that produced in specimens retrofitted with GFRP bars (i.e. G-Gr-0.1-8) (Fig. 7e), which were flexural cracks in specimen A and combined flexural and shear in B and C, broke through the adhesive line and crossed to the other side of the specimens and continued their progression into through concrete substrate, which did not happen in the BFRP-retrofitted specimens (i.e. B-Gr-0.1-8) (Fig. 7f). Where the flexural cracks that formed in specimens A and B and the shear crack in C extended to progress next to the adhesive line at the concrete-adhesive interface border but without penetrating the adhesive line. Concrete detachment took place in B-Gr-0.1-8 -B, which did not neither in C-Gr-0.1-8 nor in G-Gr-0.1-8.

For specimens in both groups, it's noteworthy that, due to the lower mechanical properties of the BFRB bars, the BFRP-retrofitted specimens showed, generally, the most ductile behaviour,

21

which was represented by having more minor cracks around the concrete-adhesive interface before failure, than the GFRP-retrofitted ones, which in turn failed with higher number of hairline cracks than those shown when using CFRP bars, which have the highest mechanical properties.

Consequently, replacing CFRP bars with GFRP and BFRP bars in the NE-bonded specimens was found to induce a noticeable shift in failure modes, transitioning from shear into a more complex combination of shear and flexural failure modes. This significant alteration proved to be highly effective, contributing to the prevention of debonding failure, a critical consideration in retrofitting scenarios. Conversely, in the case of NMEAs-bonded specimens, transitioning from CFRP to GFRP did not result in a discernible impact on the failure mode. However, delving deeper into the analysis, the shift to GFRP reinforcement within the NMEAs-bonded specimens unravelled a distinct flexural failure mode, characterized by concrete crushing phenomena. This unexpected observation underscores the nuanced interplay between different reinforcement types, unveiling varying failure behaviours and responses to applied stresses.

(a)

(b)

(c)

(d)

23

(e)

(f)

Fig. 7. Failure modes of specimens (a) C-NE-8, (b) G-NE-8, (c) B-NE-8, (d) C-Gr-0.1-8, (e) G-Gr-0.1-8 and (f) B-Gr-0.1-8.

3.2.2 The effect of bonding agent type
Overall capacities and ductility response

The comparison begins with the C-NE-8 with those bonded with the NMEAs. Using the CNF-modified epoxies led to a significant drop of about 37% in the specimens' capacities. This could be due to potentially poor dispersion of the CNF into epoxy, which caused the formation of agglomerates within the epoxy body, as shown in Fig. 5a. Only 0.1 wt.% was high enough to allow the particle-to-particle interaction instead of the intended particle-to-polymer interaction. Once it reaches this state, the particles begin to agglomerate forming clusters, which ultimately affect the Van der Waals interaction between the polymer chains, reduce the cross-linking and increase (about 20%) the void content of the matrix (i.e. porosity) (Table 5) in the nanocomposite. The resulting mechanical properties are therefore degraded. Furthermore, the agglomerations and the high void ratio are also expected to lead to a weak interface between nanoparticles and epoxy due to stress concentration at the areas of agglomerations, resulting in poor interfacial stress transfer. This eventually impaired the bonding between adhesive and concrete substrate. Moreover, due to the cotton-like nature of the CNF and its high volume-to-weight ratio, using such materials leads to thicker adhesive layer, which yielded a decrease in the adhesion properties, as confirmed in [18], which eventually led to a premature failure. Moreover, the low SSA (as shown in Table 3) of the CNF could limit the interaction between the nanoparticle with the matrix, which in turn contributed to a weaker interfacial bonding and resulted in poor stress transfer, which ultimately deteriorated the overall capacity of the specimen.

About 9% capacity drop was observed for specimens bonded with cellulose-epoxy nanocomposites. This was attributed to the particles' agglomeration alongside the huge increase (about 34%) in the % porosity compared to the NE, that would negatively impact the interfacial adhesion and therefore the stress transfer, as they act as "contraindications" for particle-matrix bonding, and they are also considered as stress concentration generators. All these reasons would influence the interfacial adhesion, and ultimately the overall performance of the retrofitting system.

On the other hand, a capacity increase of about 15% was observed in the specimens retrofitted using graphite-modified epoxies. These improvements were apparently due to the uniform dispersion of the nanoparticle into matrix preventing the formation of agglomeration, which in turn enhanced the interfacial adhesion between epoxy and the nanoparticle, leading to a higher effective interfacial area in the composite. This good bonding leads to an improvement in

mechanical properties the nanocomposites, as confirmed in [21], which reflected on the interfacial bonding with FRP reinforcement and concrete, leading to the improved performance.

Furthermore, the high SSA of the graphite nanoparticles, due to their high aspect ratio, provided a huge surface area to interact with the matrix, leading to a higher effective interfacial area in the composite, resulting in efficient stress transfer from matrix to particles ant to matrix, enhancing the interfacial adhesion between the matrix and the particle and hindering in polymer chain mobility [21], and eventually improving the mechanical properties of the matrix. Moreover, the uniform dispersion of graphite nanoparticles within the epoxy matrix as shown in Fig. 4a of the graphite-epoxy nanocomposites indicates the good compatibility between the nanoparticles and the epoxy matrix in addition to the rough surface of the nanocomposite, which made the crack propagation difficult and less prone to breakage. Moreover, the significant decrease in the void content by about 31% also expected to reduce the stress concentration and provides more uniform stress transfer. All the previous reasons would contribute to the good performance of the nanocomposites under mechanical loading, which reflected on the overall performance of the retrofitting process.

About 17% and 5% capacity increase, respectively was observed in the specimens retrofitted using silica- and clay-modified epoxies. The capacity enhancement in the silica specimens was attributed to the uniformly dispersed nanoparticles over the entire body of the matrix, as shown in Fig 5a, which in turn provided strength for the Nano-phased composites and eventually translated into improved mechanical properties, as confirmed in [22]. The reduction in void content of the matrix by about 14% in addition to the increased crystallinity gave rise to a more compact Nano-phased composites, leading, ultimately, to the enhanced mechanical performance (flexural capacity in this context). Inherent toughening properties of the Nano-silica may also contribute to increasing the strength of the epoxy adhesive [14]. Moreover, the high SSA of the silica nanoparticles could also contribute to the improved performance, due to similar reasons mentioned earlier (i.e. in the graphite specimens).

The enhancement in the mechanical properties of the epoxy by the addition of the clay nanoparticles was reflected on the overall capacities of the retrofitted specimens. It was found that filling the matrix with clay nanoparticles would ensure more viable sites for polymer and nanoparticles interaction [23]. Nano clays are dispersed in epoxy, ring-opening reactions took place followed by higher crosslinking between epoxy molecules, which resulted in interlocking resin-nanoparticles structure in the matrix and might improve the interfacial bonding strength,

facilitating stress transfer when loaded, enhancing the mechanical properties (i.e. strain at failure) of the matrix. Further explanation was provided by Huttunen-Saarivirta et al. [31] that the homogeneous dispersion of the clay nanoparticles within epoxy, which led to the interfacial bond strength between the nanoparticles and the matrix, showed an improved tensile strength and elongation at break, which (the latter) best reflected the uniformity of stress distribution. Moreover, Shi et al. [32] reported that the addition of the clay nanoparticles to epoxy matrix led to more integrated micro- and Nano-structures, through occupying the free volume, such as voids and defects that yields enhanced cross-linking density and crystallinity, improving in the mechanical properties of the matrix. In addition to that, the very high SSA of the clay nanoparticles alongside the 10% porosity reduction could also contribute to the enhanced performance, as explained earlier in the case of the silica specimens. On the other hand, although the particles aggregations showing in the clay nanocomposites (Fig. 5a) did not contribute to decrease the capacity, but they hindered achieving higher ductility enhancement. This was because of similar justifications to that reported previously.
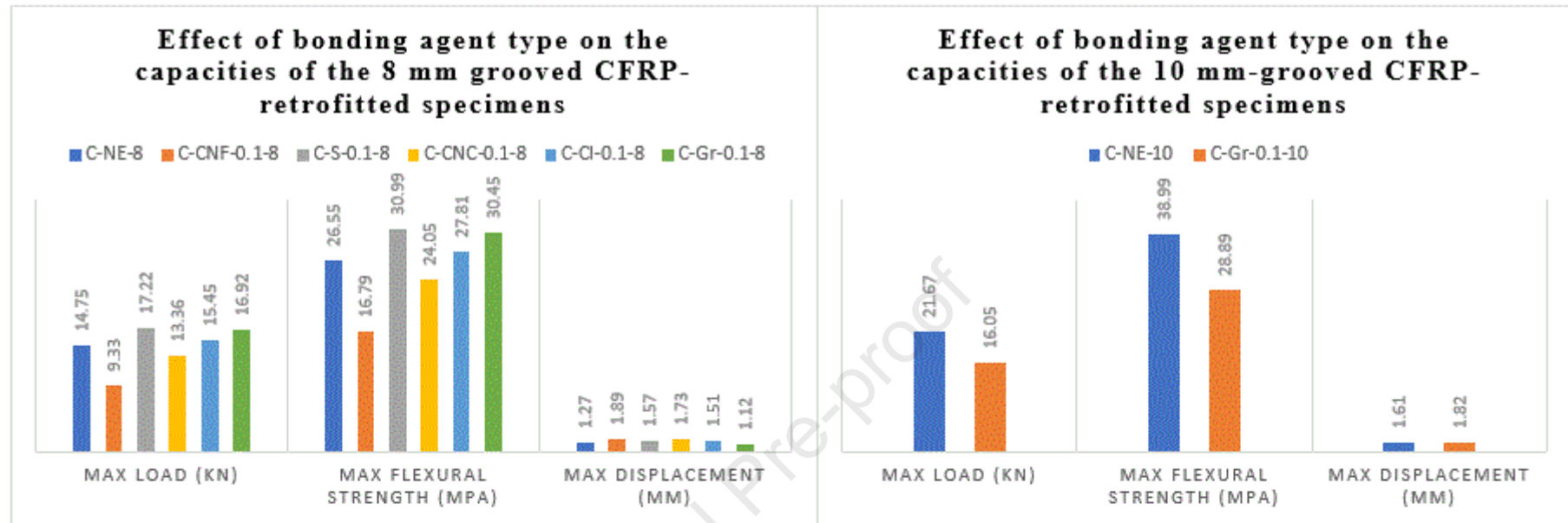
Using epoxy filled with CNF and cellulose yielded, respectively about 49% and 36% ductility increases compared to using NE, which could likely be driven by plasticization of epoxy cross-link network domains, in addition to the decreased crystallinity, which would provide the polymer chains with more freely movement. In contrast to that, about 12% reduction was observed in the graphite specimens, which could be due to the stiffening effect of graphite nanoparticles on the epoxy, which would limit the deformation capacity [14], which could also be due to its increased crystallinity.

On the other hand, ductility of specimens bonded by silica and clay-modified epoxies was found to increase by about 19% and 24%, respectively compared to the NE-bonded ones. This may be ascribed to the same mechanism took place for the enhanced strength, as discussed previously. Additionally, the silicon-based nanoparticles can help redistribute stresses during mechanical loading. Hence, these nanoparticles may act as stress transfer mediators, redistributing stress from the polymer matrix to the nanoparticles, thereby preventing localized failure and enhancing overall ductility.

In contrast with that was observed in specimen C-Gr-0.1-8 compared to its control version (i.e. C-NE-8), specimen C-Gr-0.1-10 showed about 35% capacity decrease with accompanying ductility increase of approximately 13% compared to C-NE-10. The reason for this is still unclear. On the other hand, it was observed that, compared to the control specimen (C-NE-12),
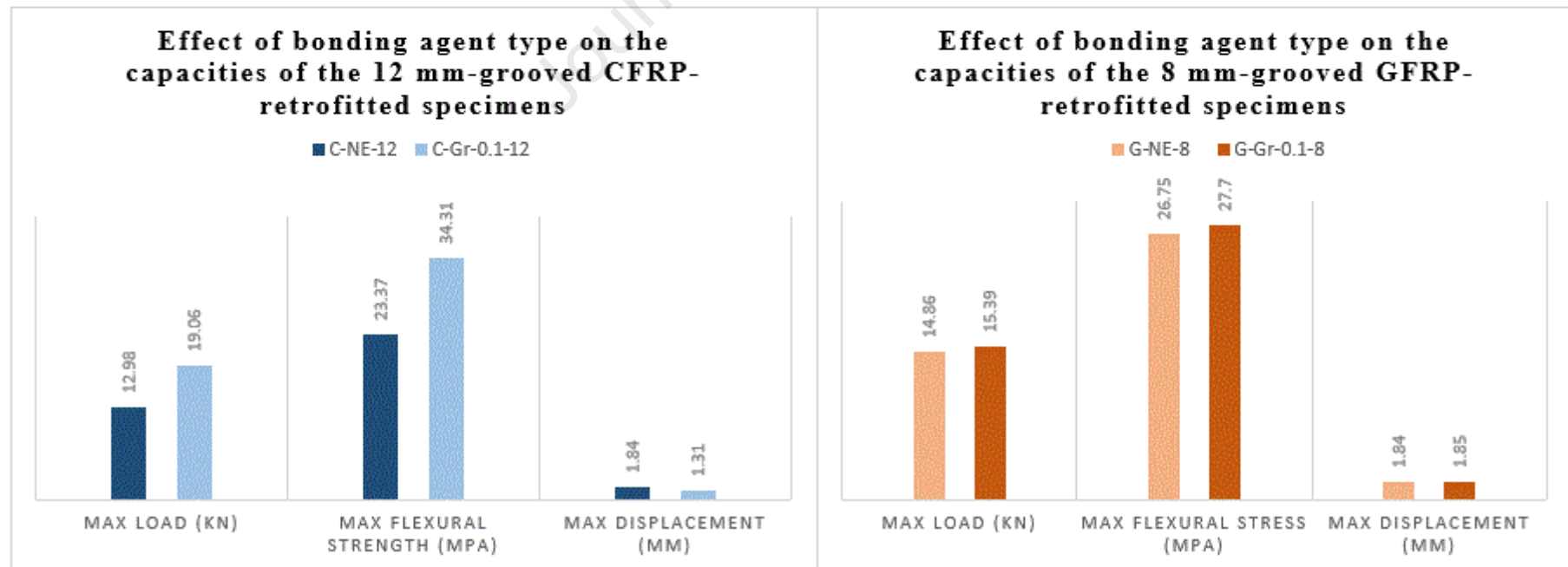
27

C-Gr-0.1-12 showed about 47% capacity increase with, conversely, about 29% ductility drop. Both capacity increase and ductility decrease could be due to the same reasons mentioned previously (i.e. in C-Gr-0.1-8).

For the GFRP-retrofitted specimens, which were bonded with NE or graphite-modified epoxy at 0.1 wt.%, it was found that using the modified adhesive yielded a slight increase in the ultimate load and displacement of about 4% and 1%, respectively over that bonded using NE, while for those retrofitted with BFRP bars, only about 2% enhancement in the load-capacity was observed, however, the ductility decreased by about 2%. Fig. 8 represents the test results of the CFRP- (a, b and c), GRRP- (d) and the BFRP- (e) retrofitted specimens, respectively.
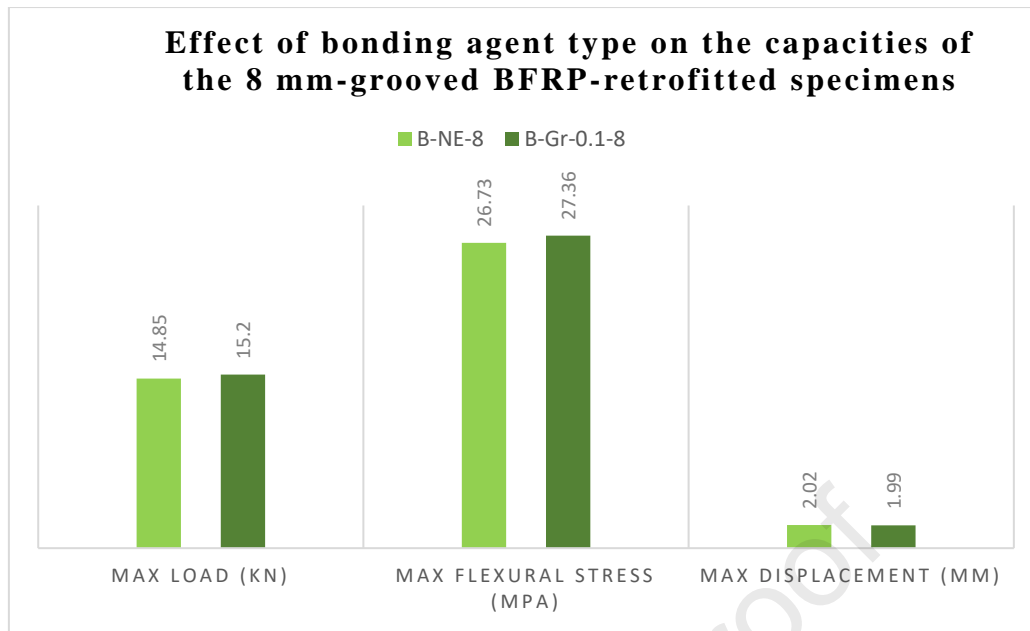
(a)

(b)

(c)

(d)

Effect of bonding agent type on the capacities of the 8 mm-grooved BFRP-retrofitted specimens

■ B-NE-8　■ B-Gr-0.1-8

(e)

Fig. 8. Effect of the type of the bonding agent on the capacities of the (a) 8 mm-grooved, (b) 10 mm-grooved, (c) 12 mm-grooved CFRP- retrofitted specimens, (d) 8 mm-grooved GFRP- and (e) BFRP-retrofitted specimens.

Failure modes

It can be seen that C-NE-8 mainly failed due to shear cracks that arose into concrete and epoxy layer, in addition to CFRP bar slippage that occurred in specimen B. C-CNF-0.1-8, which was retrofitted with CNF-modified epoxy, failed in flexure (i.e. A and B), as the adhesive layer was not strong enough to stop the crack from crossing it, which also passed to the other side. A mixed shear and flexural failure were noticed in specimen C, where the shear cracks led to partial concrete crushing accompanied by cohesive failure in the adhesive layer, which was due to, as reported earlier, the particles' agglomeration that negatively influenced the bond at the interface. So, the adhesive remained fully attached to the concrete substrate and to the CFRP bar, and no debonding took place. Bonding CFRP by epoxy-CNC nanocomposites led specimen C-CNC-0.1-8 to fail in shear, with more minor cracks showing up on the concrete surface. The shear cracks caused small parts of concrete to peel off, but no debonding was detected. For specimen C-Gr-0.1-8, that was bonded with graphite nanocomposite, a shear failure in specimens A and C, represented by a major shear crack, appeared in the concrete body with a short tail continued to align with the adhesive line. Specimen B exhibited a similar failure mode, but with smaller (i.e. less wide) shear crack, which gave the opportunity to the flexural crack to generate, which had longer tail lying on the edge of the adhesive line, but without breaking through it.

30

The C-S-0.1-8 that was retrofitted with CFRP alongside silica-modified epoxy mainly failed in shear, where the shear crack that passed through concrete and aligned with the concrete-adhesive interface could be curbed by the adhesive layer. More importantly, the shear cracks in specimen A had long tails aligning with the adhesive line, causing minor debonding failure at the bar-epoxy interface accompanied with cohesive failure. However, a stronger bond at the interfaces can be seen in specimens B and C, as no debonding was observed. Some minor cracks, especially in specimen C, appeared on the concrete surface. For specimen C-Cl-0.1-8 that was retrofitted using epoxy-clay nanocomposites, all specimens generally failed due to shear cracks, which had long extensions in specimens A and B aligning with the adhesive line from both sides of the specimens yielding a cohesive failure escorted with partial concrete crushing. The shear crack in specimen C, which failed at the highest ultimate load, was not able to affect the interfaces and its tail could not extend long beside the adhesive line.

For the 10-mm-grooved specimens, it was noticed that the shear failure was the governing failure mode in specimen C-NE-10, where almost the same failure modes took place in specimens A and B, as a main shear crack produced in the middle of the specimens from the bottom and kept progressing to break through the epoxy layer with a short tail along the edge of the epoxy line until, eventually, broke through it to the other side. Similar details were observed in specimen C, but one more shear crack generated with longer tail, but it kept beside the epoxy line without passing through it. No debonding was remarked in any of the specimens. Specimen C-Gr-0.1-10 failed in shear, similarly to what was observed in the C-NE-10, but more minor cracks appeared on the concrete surface at failure, which is linked to the failure with higher ductility. Furthermore, the main crack was observed to break through the adhesive line, leading to minor concrete crushing in A and B.

The specimen C-NE-12 (A, B and C) failed in shear, where a major shear crack began created and progressed through concrete without breaking through the adhesive layer, it leading, eventually, to minor concrete crushing. Some additional cracks also generated in specimens A and C. Bonding the CFRP reinforcement with epoxy modified with 0.1 wt.% graphite (i.e. specimen C-Gr-0.1-12) resulted in a pure shear failure mode. One main shear crack was produced in specimens A and C, while multiple cracks were found to generate in specimen B. The adhesive line was not able to curb the cracks from progressing, where they could penetrate the adhesive line and cross it (in specimens B and C) to the other side of the specimens, which yielded concrete in specimen B to peel off and also resulted in minor debonding failure at the concrete-adhesive interface.

31

The second group to be considered, as mentioned earlier, includes the specimens retrofitted with GFRP bars alongside NE (i.e. G-NE-8) and graphite-modified epoxy (i.e. G-Gr-0.1-8). The failure modes of both specimens were previously discussed. Specimens G-NE-8-A, B and C failed due to flexural crack that broke through the epoxy layer leading it to peel off at the bar-epoxy interface in specimen A. Crushing of a part of concrete was also observed in specimens A and B. For G-Gr-0.1-8, flexural failure was noticed in A, while a combined flexural and shear failure mode occurred in B and C. The cracks were observed to penetrate the adhesive line to the other side of the specimens and continued their way into through concrete, but with no debonding at the interfaces or concrete detachment. Therefore, in the GFRP-retrofitted specimens, using graphite-modified epoxy adhesive instead of NE could enhance the bond at the interfaces, as no debonding mode of failure or concrete detachment took place.

The BFRP-retrofitted specimens alongside NE (i.e. B-NE-8) and graphite-modified epoxy (i.e. B-Gr-0.1-8) are comprised in the third group. Modes of failure of both specimens are included in a previous section. In specimens B-NE-8-A and B, a mixed shear and flexural failure mode was observed, where main flexural crack alongside minor shear crack extended to align with the adhesive line at the concrete-epoxy interface. In specimen A, the crack was noticed to further progress leading parts of concrete to peel off with thin layers of epoxy stuck on them. Specimen C mainly failed in shear, but the shear cracks did not align with the epoxy line, but alternatively crossed it only in one place. Moreover, the epoxy line could limit the crack to progress to the other end of the specimen. For specimens B-Gr-0.1-8, the flexural cracks that formed in specimens A and B and the shear crack in C extended to progress next to concrete-adhesive interface border but without penetrating the adhesive line. So, it can be concluded that using the graphite-modified adhesive rather that NE, in the BFRP-retrofitted specimens, contributed to a stronger bond at the concrete-adhesive interface, as no cracks could break through the adhesive line at the interface. Fig. 9 shows the failure modes of the rest of the specimens that were considered to investigate the effect of the bonding agent type.
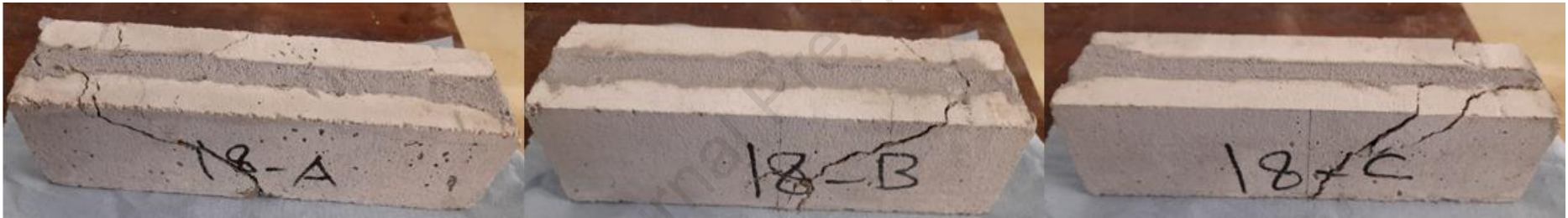
(a)

(b)

(c)

33

(d)

(e)

(f)

(g)

(h)

Fig. 9. Failure modes of specimens (a) C-CNF-0.1-8, and (b) C-S-0.1-8, (c) C-CNC-0.1-8, (d) C-Cl-0.1-8 (e) C-NE-10, (f) C-Gr-0.1-10, (g) C-NE-12 and (h) C-Gr-0.1-12.

35

3.2.3 The effect of the nanoparticles used in the NMEAs

Overall capacities and ductility response

First, for the specimens bonded with epoxy adhesive loaded with carbon-based nanoparticles, e.g. CNF, cellulose and graphite, the specimens retrofitted using epoxy modified with graphite showed the best performance compared to the ones loaded with CNF and cellulose nanocomposites, resulting in about 81% and 27% higher ultimate loads, respectively compared to those retrofitted with CNF- and cellulose-modified epoxies. This could be due to (I) the highest % crystallinity accompanied with the lowest % porosity and (II) the agglomeration-free appearance seen in the graphite nanocomposites alongside the rough surface of the nanocomposite. The non-formation of the agglomerations could be due to the higher SSA of the graphite nanoparticles compared to those of the other nanoparticles, which could contribute to the uniform dispersion of the particles within the adhesive body, resulting in the better performance. Moreover, the highest density of the graphite particles among the carbon-based particles could lead to "densify" the nanocomposites, minimizing the pores in the adhesive body, that act as stress concentration areas and facilitate the crack propagation, providing more favourable stress transfer and better mechanical performance.

The specimens retrofitted with cellulose nanocomposites failed at about 43% higher ultimate load than that bonded by CNF nanocomposites. This was because of the CNF particles, as shown in Fig. 6a, were agglomerating in larger clusters within the adhesive body compared to the small agglomerating cellulose particles that were scattered throughout the adhesive body. Therefore, the gathering of agglomerates in the form of large bundles, as shown in the CNF, could eventually lead to higher stress concentration and less efficient stress transfer process, deteriorating the interfacial bond strength, that directly affected the capacities of the specimens. Furthermore, the better performance provided by the cellulose nanocomposites could also be due to the powder nature of the cellulose nanoparticles rather than the cotton-like nature of the CNF nanoparticles, which had a negligible effect on the thickness of the adhesive layer and eventually on the adhesion strength.

It is noteworthy that although the cellulose nanoparticles have lower SSA and density than the CNF, which were expected to better enhance the performance of the specimens bonded with the CNF-epoxy than those bonded with cellulose nanocomposites, the reasons mentioned above seem to have "stronger" impact in lowering the specimens' capacities. However, the effect of the better physical properties alongside the higher % crystallinity of the CNF nanocomposites compared to those of the cellulose might reflect on the ductility response, as the specimens

bonded with CNF nanocomposites were more ductile showing about 9% higher ductility at failure than those bonded with cellulose-modified epoxies. It was also observed that the latter were about 35% more ductile than those bonded with graphite nanocomposites, which showed about 41% more brittle behaviour than those bonded with the CNF nanocomposites, which could be ascribed to the high % crystallinity, which is known to increase the brittleness of the composite, as discussed earlier.

Second, in regard with using epoxy filled with silicon-based nanoparticles (i.e. silica and clay), even though the SSA of the Nano clay is much higher than that of the silica particles, which have also less density, lower capacities and ductility were obtained with the specimens bonded with the clay nanocomposites. The specimens bonded using silica-modified epoxy exhibited about 11% and 4% increase in the capacity and ductility, respectively over those bonded with clay NMEAs. This could be due to that the size of the silica nanoparticles, as shown in Table 3, is about 50 times smaller than that of the clay ones, which led the silicon particles to disperse more uniformly within the epoxy preventing the formation of agglomeration unlike what was observed in the clay nanocomposites, leading to enhanced interfacial bonding and resulting in more efficient interfacial stress transfer, which ultimately yielded better overall performance. The higher crystallinity and lower % porosity of the silica nanocomposites also contributed to the better behaviour.

Higher increase of capacity resulted from the silicon-based nanocomposites could be due to the lower % porosity and the higher % crystallinity. This behaviour could be also due to the fact that the van der Waals interactions between molecules are much stronger in the carbon-based materials, especially in the CNF, causing them to aggregate into entangled bundles that prevent the formation of uniform and optimal materials [19]. This would eventually lead to that the nanoparticles would not be able to provide the epoxy with their ultimate enhancement capacity, which ultimately cannot be fully utilised. However, using carbon-based nanoparticles could improve the specimens' ductility slightly more than that in the case of using the silicon-based ones, which could be owing to their lower % crystallinity.

Consequently, it was found that the specimens bonded with epoxy modified with silicon-based nanoparticles showed, on average, about 24% higher capacities than those bonded using epoxy loaded with carbon-based nanoparticles, which, on the other hand, showed about 3% more ductile behaviour.

A comparison between using the carbon-based and the silicon-based nanocomposites, as bonding agents, in terms of specimens' capacities and the ductility is shown in Fig. 10.
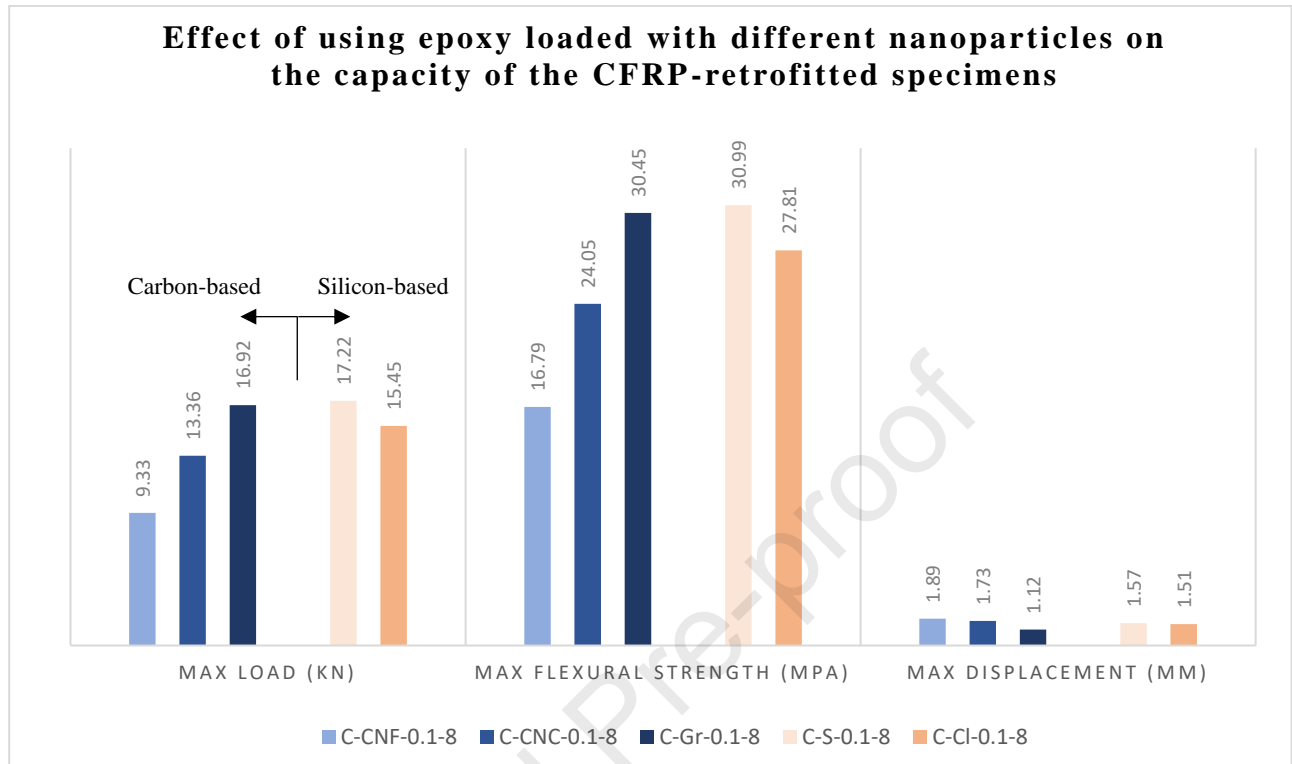

Fig. 10. Effect of using different nanoparticles in the NMEAs on the capacities of the CFRP-retrofitted specimens.

Failure modes

The failure modes were previously discussed in detail in section 3.2.2. It was found that the specimens retrofitted using silicon-epoxy nanocomposites mainly failed in shear, while a mixed shear and flexural failure mode was observed in those retrofitted using carbon-epoxy nanocomposites. Moreover, the debonding at bar-adhesive interface (i.e. bar slippage) could be avoided by using epoxy reinforced with carbon-based nanoparticles, while using epoxy loaded with silicon-based nanoparticles was not able to prevent the debonding failure, which happened at the bar-epoxy interface with using silica-epoxy nanocomposites.

3.2.4 The effect of the wt.% concentration of the nanoparticles (graphite)

Overall capacities and ductility response

Graphite nanoparticles, as a representative, were employed to further study the effect of the wt.% concentration, that is, the epoxies filled with 0.2 and 0.3 wt.% graphite nanoparticles were used to bond the concrete specimens prepared for that purpose. It can be seen that capacities decreased with increasing the wt.% concentration of the nanoparticle used to prepare the nanocomposites.

Where about 3% and 36% capacity reduction were observed, respectively with doubling (i.e. 0.2 wt.%) and tripling (i.e. 0.3 wt.%) the graphite wt.% incorporated into epoxy. In addition, increasing the graphite wt.% from 0.2 to 0.3 wt.% decreased the capacity by about 34%. The capacity drop took place with the wt.% was ascribed to multiple reasons; (I) the increasing agglomerations with the concentration, as shown in Fig. 7, that, as discussed previously in more detail, could deteriorate the adhesion properties of epoxy, which weakened the interfacial bond yielding premature failure of the specimen, (II) the increase in the % porosity by about 8% and 61%, respectively with doubling and tripling the wt.%, which also negatively affected the performance, as discussed in section 3.2.2, and (III) the increased crystallinity which has its effect explained previously, which in turn led the specimens' ductility response to improve, where doubling and tripling the wt.% resulted in about 11% and 21% ductility increase, respectively, while moving from 0.2% to 0.3% enhanced the ductility by about 7%. Fig. 11 represents the effect of the wt.% of the graphite nanoparticles on the capacities of the CFRP-retrofitted specimens.
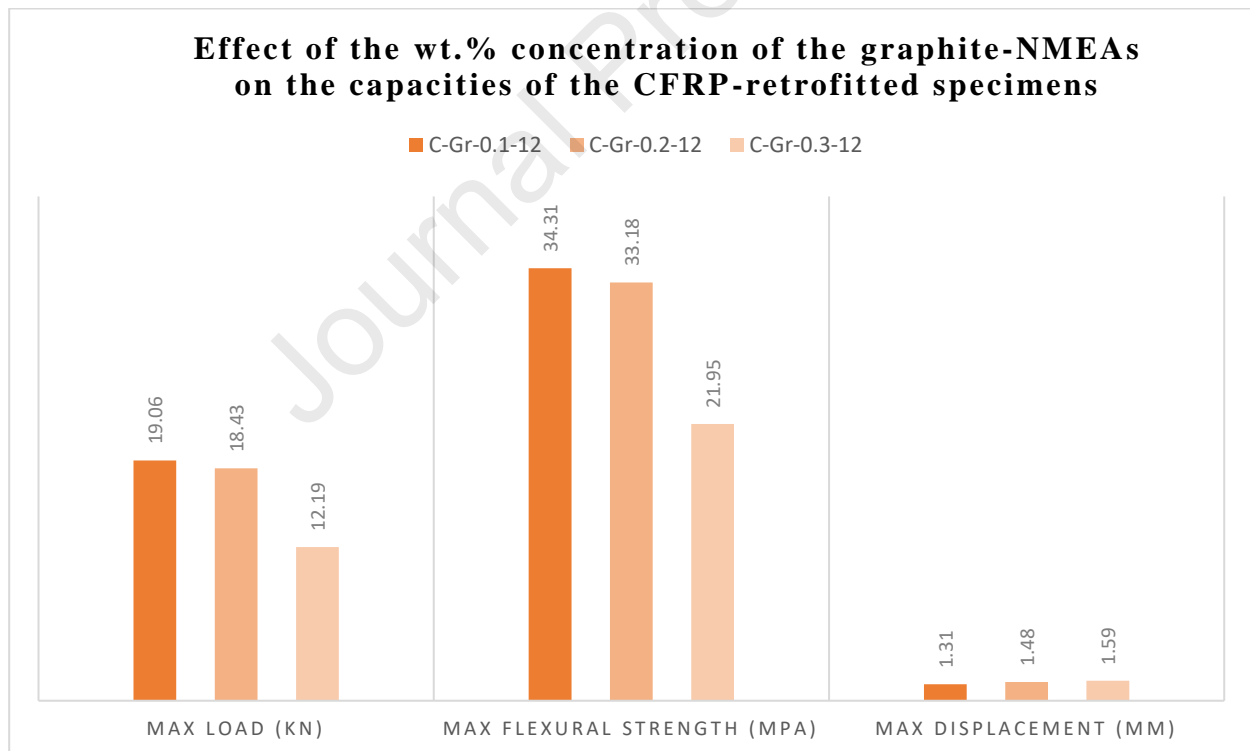

Fig. 11. Effect of graphite NMEAs wt.% concentration on the capacities of the CFRP-retrofitted specimens.

Failure modes

Specimen C-Gr-0.1-12, as discussed in section 3.2.2, failed due to pure shear failure mode. Using epoxy loaded with 0.2 wt.% of graphite led specimen C-Gr-0.2-12 to fail in a similar mode to that of C-Gr-0.1-12, but in a more ductile way, as more minor cracks showed up at failure. Moreover, no debonding failure or concrete detachment took place. Finally, specimens C-Gr-0.3-12-A, B and C failed due to shear cracks, which led to partial concrete crushing. However, the adhesive line was strong enough to prevent the cracks from penetrating it, since these specimens (i.e. C-Gr-0.3-12 B and C) showed the most ductile behaviour compared to the previous ones (i.e. C-Gr-0.1-12 and C-Gr-0.2-12). Compared to using NE (C-NE-12), bonding the specimens with the NMEAs could minimise the concrete crushing failure, even though it reduced the ductility. The failure modes of specimens C-Gr-0.2-12 and C-Gr-0.3-12 are illustrated in Fig. 12.

(a)

(b)

Fig. 12. Failure modes of specimens (a) C-Gr-0.2-12 and (b) C-Gr-0.3-12.

41

3.2.5 The effect of groove size

Overall capacities and ductility response

Two groups of specimens were considered to study the effect of using different groove dimensions: the first group includes the specimens retrofitted with CFRP bars and bonded with NE (i.e. C-NE-8, 10 and 12), while the CFRP-retrofitted specimens bonded with graphite-0.1 NMEAs (i.e. C-Gr-0.1-8, 10 and 12) are encompassed in the second group.

It was found, in the first group, that considering the groove size 10x10 rather than 8x8 yielded a significant increase in the load-carrying capacity of the specimens and their ductility of about 47% and 27%, respectively, which disagrees with what was reported in the literature [25, 27]. Further increase in the groove dimensions (i.e. using 12x12 mm grooves) led to a capacity drop by about 14% and 67% compared to using 8x8 and 10x10 mm grooves, respectively. Nevertheless, a corresponding increase in the specimens' ductility of about 45% and 14% was remarked.
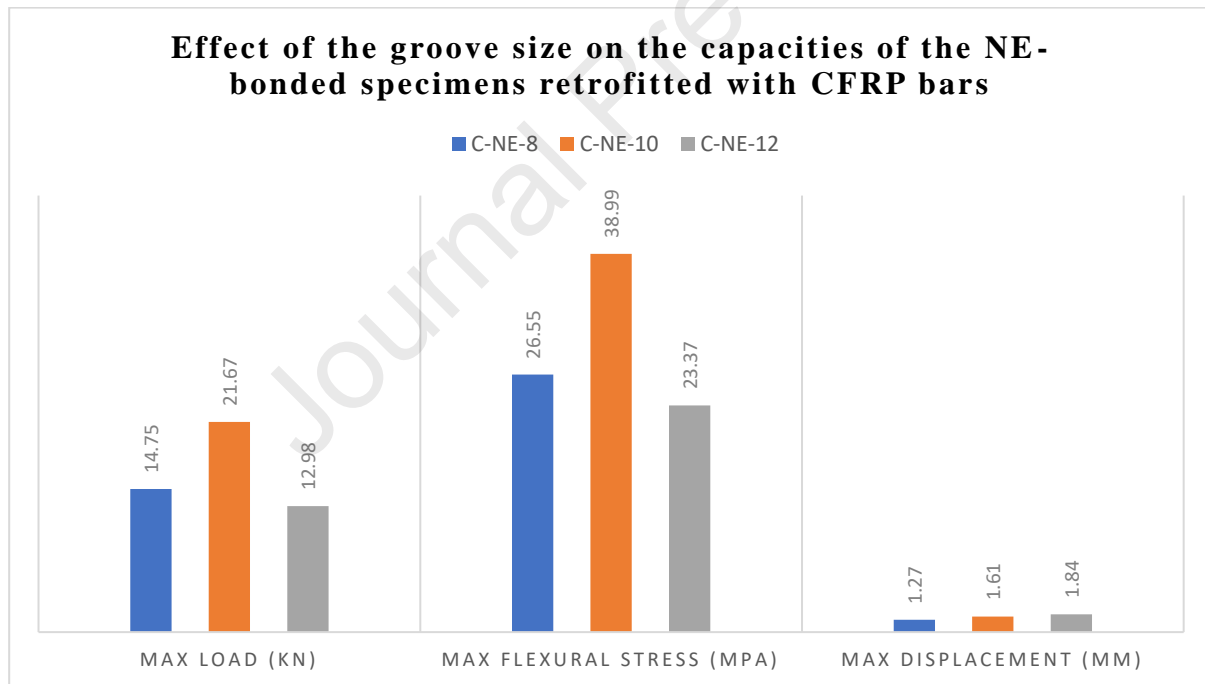
It's noteworthy that increasing the groove size with keeping the same FRP bar dimensions means that more adhesive was utilised. Thus, installing the FRP reinforcement further to the groove edge; in a bigger groove, would delay the stresses generated in the specimen from affecting the FRP-adhesive interface, which would eventually delay the failure, and end up with a higher-capacity specimen. Furthermore, it was reported by Hassan and Rizkalla [26] that increasing the thickness of the adhesive (i.e. by increasing the groove size) reduces the stress deformation within the adhesive layer, which eventually reduces the interfacial stresses. However, further increasing in the groove size resulted in a reverse effect, as a sharp drop in the capacity was reported. This might be due to that using too much adhesive generated more interfacial stresses, which negatively affected the interfacial adhesion, leading to a premature failure.

It was also detected that the ductility increased with the groove size. This could be due to that increasing the groove dimensions means increasing the distance between the grooves' sides. That the FRP bar is surrounded with more adhesive might delay the crack progression, which would take longer to cross from one side to another and cause the failure, leading ultimately to more ductile behaviour.
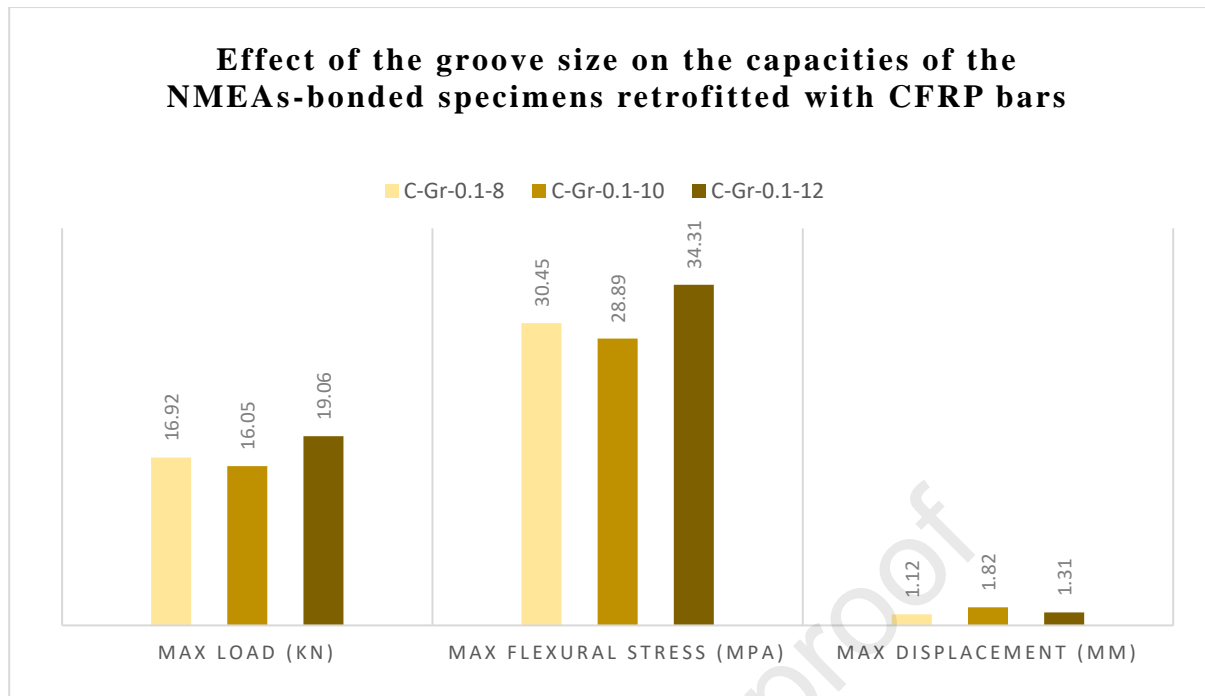
For the specimens in the second group, it was observed that increasing the groove size (in mm^3) by about 56% (i.e. from 8x8x200 to 10x10x200) decreased the load-carrying capacity of the specimens by about 5%. However, the ductility significantly increased by about 63%. While about 13% and 17% increases in the capacity and ductility, respectively were observed with

about 125% increase in the groove size (i.e. from 8x8 mm to 12x12 mm). The greatest increase in the capacity of about 19% was found when moving from 10x10 to 12x12 mm groove dimensions, with a corresponding increase in the groove size of about 44%. Nevertheless, about 28% reduction in the specimens' ductility was noticed.

Therefore, it could be observed that a non-monotonic trend in the load-carrying capacity took place with changing the groove dimensions from 8x8 to 10x10 and to 12x12 mm. However, it could be seen that the increasing the groove dimensions resulted in a clearer trend in the specimens' ductility, as it increased with moving from 8x8 to 10x10 and to 12x12 mm. This could be due to the same reasons observed in the first group. Nevertheless, ductility decrease was reported with moving from 10x10 to 12x12 mm. It could be concluded, as previously observed, that there is an inverse relationship between the change in the load capacity and the ductility with moving from 8x8 to 10x10 and to 12x12 mm groove dimensions, as shown in Fig. 13.

(a)

Effect of the groove size on the capacities of the NMEAs-bonded specimens retrofitted with CFRP bars

(b)

Fig. 13. Effect of groove size on the capacities of the CFRP-retrofitted specimens bonded with (a) NE and (b) graphite-0.1 NMEAs.

Failure modes

In the first group, the specimen C-NE-8, as discussed in section 3.2.1 and as shown in Fig. 7a, failed due to shear cracks combined with a debonding noticed in specimen B. Specimen C-NE-10 (Fig. 9e) also failed in pure shear without any other failure type noticed, which could be due to that, as reported by De Lorenzis and Nanni [29, 30], as the groove size increases, the thickness of the epoxy cover increases, which offers a higher resistance to splitting and eventually shifts the failure from epoxy to the surrounding concrete. Similar to what was observed in the previous specimens, the specimen C-NE-12 (A, B and C) (Fig. 9g), as discussed in the previous section, failed in shear followed by concrete crushing.

For the second group, specimen C-Gr-0.1-8 (Fig. 7d), which was retrofitted with 8 mm groove, failed in shear, as a major shear crack appeared in the concrete body with an extended tail continued to align with the adhesive line, but without passing through it. Considering 10 mm groove in specimen C-Gr-0.1-10 (Fig. 9f) resulted in shear failure with more sub-cracks noticed on the concrete surface, which could be due to the higher ductility. Furthermore, unlike what was noticed in specimen C-Gr-0.1-8, slight concrete peeling-off was noticed in B. For specimen C-Gr-0.1-12 (Fig. 8h), which was retrofitted with 12 mm groove, and as discussed beforehand, similar failure mode to that observed in specimen C-Gr-0.1-10 was noticed, but fewer minor cracks appeared at failure. Moreover, more concrete than that happened in C-Gr-0.1-10 was detached. Therefore, it could be concluded that using smaller groove width could restrict the crack progression from breaking through adhesive line, and eventually was able to prevent the concrete peeling-off. This could be ascribed to that using smaller groove dimensions would result in less stress concentration at the interfaces. This is because of that increasing the groove dimensions means surrounding the FRP bar and bonding the concrete substrate with more adhesive, leading to higher interfacial stress concentration and weaker bonding at the interfaces.

Consequently, for the NE-bonded specimens, almost the same failure modes (i.e. pure flexure) were observed in all specimens. Thus, it can be concluded that altering the groove dimensions had insignificant influence on the failure modes, as it did not contribute in resisting the crack progression at all.

Unlike what occurred in the case of using 10 mm and 12 mm groove dimensions, considering 8 mm grooves in the NMEAs-bonded specimens was able to curb the crack progression by preventing it from passing through the adhesive line. Moreover, no concrete peeling-off took place in the 8-mm-grooved specimens dissimilar to what happened in the other ones.

45

4. Conclusions

The efficiency of the NMEAs-bonded NSM-FRP technique for the flexural retrofitting of concrete was examined and achieved through a comprehensive experimental and characterisation (i.e. SEM and XRD analyses) programme. Concrete prisms were tested under three-point bending for their load-carrying capacities and ductility response. Their structural failure modes were also monitored. From the obtained results, the following main conclusions could be drawn:

- The CFRP-retrofitted concrete bonded with the graphite-modified epoxies showed capacity increase of about 10% and 12%, respectively compared to the ones retrofitted with the GFRP and the BFRP bars. Furthermore, about 44% and 8% higher ductility were observed in the BFRP-retrofitted than the CFRP and GFRP-retrofitted concretes, respectively.

- Moving from CFRP to GFRP and to BFRP in the NE-bonded retrofit altered the failure mode from shear to flexural and to combined shear/flexural, and could avoid the debonding failure, while moving from CFRP to GFRP in the NMEAs-bonded specimens had no effect on the failure mode, but moving to BFRP showed a flexural failure followed by concrete crushing.

- Compared to specimens bonded with NE, using CNF and cellulose NMEAs reduced the capacities by about 37% and 9%, respectively, which was due to the weak interfacial bonding caused by particles' agglomeration and the high % porosity of the produced nanocomposites. Nevertheless, significant ductility increases of about 49% and 36% were achieved.

- Bonding specimens with silica-, clay- and graphite-modified epoxies resulted in capacity increases of approximately 17%, 5% and 15%, respectively, over those bonded with NE. However, the higher crystallinity of the graphite nanocomposites led to about 12% ductility reduction in the graphite-epoxy-bonded specimens, while using silica and clay nanocomposites resulted in about 19% and 24% ductility enhancement, respectively.

- Bonding the 10-mm-grooved specimens with 0.1 wt.% graphite nanocomposites (i.e. C-Gr-0.1-10) decreased the capacity by about 35% but increased ductility by approximately 13% compared to those bonded with NE (i.e. C-NE-10). While about 47% capacity increase with about 29% ductility reduction were observed in the 12-mm-grooved specimens (i.e. C-Gr-0.1-12).

- Using epoxy filled with carbon-based nanoparticles rather than NE was able to prevent the interfacial debonding and switched the failure mode, as occurred in C-CNF-0.1-8, from shear to flexural. While slight debonding at the bar-adhesive interface was observed in the specimens retrofitted using silicon-based NMEAs (i.e. silica nanocomposites) accompanied

46

with cohesive failure in the adhesive layer alongside minor concrete crushing. However, the concrete-adhesive interfacial bonding could be kept intact and the shear failure mode was maintained.

- The specimens retrofitted with silicon-based NMEAs predominantly failed in shear, whereas a mixed shear and flexural failure modes were exhibited by those retrofitted with carbon-epoxy NMEAs.

- Using the graphite NMEAs rather than NE to bond the 10- and the 12-mm-grooved specimens had insignificant effect on the failure modes.

- The capacities of NMEAs-bonded retrofitted concretes decreased as the wt.% concentration of the nanoparticles (i.e. graphite) increased because of nanoparticles' agglomeration within the epoxy body beside the increase in the void content and the crystallinity decrease. However, a ductility enhancement with the concentration was observed.

- Bonding specimens with epoxy filled with nanoparticles at different wt.% did not influence the failure modes, where all specimens mainly failed in shear.

- Increasing the b/d_b ratio from 1.33 to 1.67 in the NE-bonded specimens led to about 47% and 27% increases in the specimens' capacities and their ductility, respectively, while moving from 1.33 to 2.00 yielded about 14% capacity drop, but a ductility increase of about 45% was achieved. Whereas about 5% decrease capacity decrease, but a ductility increases of about 63% was reported when moving from 1.33 to 1.67 in the NMEAs-bonded specimens. Further increase in the b/d_b ratio (i.e. from 1.33 to 2.00) yielded increases in both capacity and ductility by about 13% and 17%, respectively.

- Using 10 mm and 12 mm grooves could prevent the debonding mode, which was observed in the 8-mm-grooved specimens bonded with NE. However, the shear failure was the dominant in all specimens. All the NMEAs-bonded specimens mainly failed due to shear cracks, followed by concrete crushing observed in the 10- and 12-mm-grooved specimens.

- A consistent correlation was observed between the SEM and the XRD results, where the NMEAs specimens with high agglomeration and high % porosity had low values of % crystallinity and vice versa. These characteristics had a direct effect on the mechanical behaviour of the nanocomposites in the retrofitting system.

Data availability

The data supporting the findings of this study is entirely contained within this paper. All data used for analysis is presented in the main text of this paper. No external or additional data sources were utilized in this study. The data can be accessed upon request from the corresponding author.

References

[1] Irshidat, M.R., Al-Saleh, M.H. and Almashagbeh, H., 2016. Effect of carbon nanotubes on strengthening of RC beams retrofitted with carbon fiber/epoxy composites. *Materials & Design*, *89*, pp.225-234 [DOI: https://doi.org/10.1016/j.matdes.2015.09.166].

[2] Irshidat, M.R. and Al-Saleh, M.H., 2016. Effect of using carbon nanotube modified epoxy on bond–slip behavior between concrete and FRP sheets. *Construction and Building Materials*, *105*, pp.511-518 [DOI: https://doi.org/10.1016/j.conbuildmat.2015.12.183].

[3] Al-Zu'bi, M., Fan, M. and Anguilano, L., 2022. Advances in bonding agents for retrofitting concrete structures with fibre reinforced polymer materials: A review. *Construction and Building Materials*, *330*, p.127115 [DOI: https://doi.org/10.1016/j.conbuildmat.2022.127115].

[4] Abdullah, S.R., Rosli, F.N., Ali, N., Abd Hamid, N.A. and Salleh, N., 2020. Modified Epoxy for Fibre Reinforced Polymer Strengthening of Concrete Structures. *International Journal of Integrated Engineering*, *12*(9), pp.103-113 [DOI: https://doi.org/10.30880/ijie.2020.12.09.013].

[5] Liu, S., Chevali, V.S., Xu, Z., Hui, D. and Wang, H., 2018. A review of extending performance of epoxy resins using carbon nanomaterials. *Composites Part B: Engineering*, *136*, pp.197-214 [DOI: https://doi.org/10.1016/j.compositesb.2017.08.020].

[6] Al-Zu'bi, M., Fan, M., Al Rjoub, Y., Ashteyat, A., Al-Kheetan, M.J. and Anguilano, L., 2021. The effect of length and inclination of carbon fiber reinforced polymer laminates on shear capacity of near-surface mounted retrofitted reinforced concrete beams. *Structural Concrete*, *22*(6), pp.3677-3691 [DOI: https://doi.org/10.1002/suco.202100198].

[7] Johnsen, B.B., Kinloch, A.J., Mohammed, R.D., Taylor, A.C. and Sprenger, S., 2007. Toughening mechanisms of nanoparticle-modified epoxy polymers. *Polymer*, *48*(2), pp.530-541 [DOI: https://doi.org/10.1016/j.polymer.2006.11.038].

[8] Quan, D., Urdániz, J.L. and Ivanković, A., 2018. Enhancing mode-I and mode-II fracture toughness of epoxy and carbon fibre reinforced epoxy composites using multi-walled carbon nanotubes. *Materials & Design*, *143*, pp.81-92
[DOI: https://doi.org/10.1016/j.matdes.2018.01.051].

[9] Ashrafi, B., Guan, J., Mirjalili, V., Zhang, Y., Chun, L., Hubert, P., Simard, B., Kingston, C.T., Bourne, O. and Johnston, A., 2011. Enhancement of mechanical performance of epoxy/carbon fiber laminate composites using single-walled carbon nanotubes. *Composites science and technology*, *71*(13), pp.1569-1578.
[DOI: https://doi.org/10.1016/j.compscitech.2011.06.015].

[10] Singh, N.P., Gupta, V.K. and Singh, A.P., 2019. Graphene and carbon nanotube reinforced epoxy nanocomposites: A review. *Polymer*, *180*, p.121724.
[DOI: https://doi.org/10.1016/j.polymer.2019.121724].

[11] Irshidat, M.R. and Al-Saleh, M.H., 2017. Flexural strength recovery of heat-damaged RC beams using carbon nanotubes modified CFRP. *Construction and Building Materials*, *145*, pp.474-482 [DOI: https://doi.org/10.1016/j.conbuildmat.2017.04.047].

[12] Irshidat, M.R., Al-Saleh, M.H. and Al-Shoubaki, M., 2015. Using carbon nanotubes to improve strengthening efficiency of carbon fiber/epoxy composites confined RC columns. *Composite Structures*, *134*, pp.523-532.
[DOI: https://doi.org/10.1016/j.compstruct.2015.08.108].

[13] Morshed, S.A., Sinha, A., Zhang, Q. and Tatar, J., 2019. Hygrothermal conditioning of wet-layup CFRP-concrete adhesive joints modified with silane coupling agent and core-shell rubber nanoparticles. *Construction and Building Materials*, *227*, p.116531.
[DOI: https://doi.org/10.1016/j.conbuildmat.2019.07.257].

[14] Morshed, S.A., Young, T.J., Chirdon, W.M., Zhang, Q. and Tatar, J., 2020. Durability of wet lay-up FRP bonded to concrete with nanomodified epoxy adhesives. *The Journal of Adhesion*, *96*(13), pp.1141-1166 [DOI: https://doi.org/10.1080/00218464.2018.1556647].

[15] Rousakis, T.C., Kouravelou, K.B. and Karachalios, T.K., 2014. Effects of carbon nanotube enrichment of epoxy resins on hybrid FRP–FR confinement of concrete. *Composites Part B: Engineering*, *57*, pp.210-218 [DOI: https://doi.org/10.1016/j.compositesb.2013.09.044].

[16] Soliman, S.M., El-Salakawy, E. and Benmokrane, B., 2010. Flexural behaviour of concrete beams strengthened with near surface mounted fibre reinforced polymer bars. *Canadian Journal of Civil Engineering*, *37*(10), pp.1371-1382 [DOI: https://doi.org/10.1139/L10-077].

[17] Abdallah, M., Al Mahmoud, F., Khelil, A., Mercier, J. and Almassri, B., 2020. Assessment of the flexural behavior of continuous RC beams strengthened with NSM-FRP bars, experimental and analytical study. *Composite Structures*, *242*, p.112127. [DOI: https://doi.org/10.1016/j.compstruct.2020.112127].

[18] Tomblin, J.S., Yang, C. and Harter, P., 2001. *Investigation of thick bondline adhesive joints*. WICHITA STATE UNIV KS.

[19] Filleter, T., Bernal, R., Li, S. and Espinosa, H.D., 2011. Ultrahigh strength and stiffness in cross-linked hierarchical carbon nanotube bundles. *Advanced Materials*, *23*(25), pp.2855-2860 [DOI: https://doi.org/10.1002/adma.201100547].

[20] ASTM, C., 2002. 78-02. Standard test method for flexural strength of concrete (using simple beam with third–point loading). *Annual Book of ASTM Standards, American Society for Testing and Materials*.

[21] Kumar, A., Chouhan, D.K., Alegaonkar, P.S. and Patro, T.U., 2016. Graphene-like nanocarbon: An effective nanofiller for improving the mechanical and thermal properties of polymer at low weight fractions. *Composites Science and Technology*, *127*, pp.79-87 [DOI: https://doi.org/10.1016/j.compscitech.2016.02.028].

[22] Chisholm, N., Mahfuz, H., Rangari, V.K., Ashfaq, A. and Jeelani, S., 2005. Fabrication and mechanical characterization of carbon/SiC-epoxy nanocomposites. *Composite structures*, *67*(1), pp.115-124 [DOI: https://doi.org/10.1016/j.compstruct.2004.01.010].

[23] Hosur, M., Mahdi, T.H., Islam, M.E. and Jeelani, S., 2017. Mechanical and viscoelastic properties of epoxy nanocomposites reinforced with carbon nanotubes, nanoclay, and binary nanoparticles. *Journal of Reinforced Plastics and Composites*, *36*(9), pp.667-684 [DOI: https://doi.org/10.1177/0731684417691365].

[24] Abdallah, M., Al Mahmoud, F., Khelil, A., Mercier, J. and Almassri, B., 2020. Assessment of the flexural behavior of continuous RC beams strengthened with NSM-FRP bars, experimental and analytical study. *Composite Structures*, *242*, p.112127 [DOI: https://doi.org/10.1016/j.compstruct.2020.112127].

[25] Barris, C., Sala, P., Gómez, J. and Torres, L., 2020. Flexural behaviour of FRP reinforced concrete beams strengthened with NSM CFRP strips. *Composite Structures*, *241*, p.112059 [DOI: https://doi.org/10.1016/j.compstruct.2020.112059].

[26] Hassan, T. and Rizkalla, S., 2003. Investigation of bond in concrete structures strengthened with near surface mounted carbon fiber reinforced polymer strips. *Journal of composites for construction*, *7*(3), pp.248-257.

 [DOI: https://doi.org/10.1061/(ASCE)1090-0268(2003)7:3(248)].

[27] Fathuldeen, S.W. and Qissab, M.A., 2019. Behavior of RC beams strengthened with NSM CFRP strips under flexural repeated loading. Structural Engineering and Mechanics, 70(1), pp.67-80.

[28] Hassan, T. and Rizkalla, S., 2004. Bond mechanism of NSM FRP bars for flexural strengthening of concrete structures. *ACI Structural Journal*, *101*(6), pp.830-839.

[29] De Lorenzis, L. and Nanni, A., 2002. Bond between near-surface mounted fiber-reinforced polymer rods and concrete in structural strengthening. Structural Journal, 99(2), pp.123-132.

[30] Lorenzis, L.D. and Nanni, A., 2001b. Characterization of FRP rods as near-surface mounted reinforcement. Journal of Composites for Construction, 5(2), pp.114-121 [DOI: https://doi.org/10.1061/(ASCE)1090-0268(2001)5:2(114)].

[31] Huttunen-Saarivirta, E., Vaganov, G.V., Yudin, V.E. and Vuorinen, J., 2013. Characterization and corrosion protection properties of epoxy powder coatings containing nanoclays. *Progress in Organic Coatings*, *76*(4), pp.757-767

[DOI: https://doi.org/10.1016/j.porgcoat.2013.01.005].

[32] Shi, X., Nguyen, T.A., Suo, Z., Liu, Y. and Avci, R., 2009. Effect of nanoparticles on the anticorrosion and mechanical properties of epoxy coating. *Surface and Coatings Technology*, *204*(3), pp.237-245 [DOI: https://doi.org/10.1016/j.surfcoat.2009.06.048].

[33] Kumar, A., S Negi, Y., K Bhardwaj, N. and Choudhary, V., 2013. Synthesis and characterization of cellulose nanocrystals/PVA based bionanocomposite. *Advanced materials letters*, *4*(8), pp.626-631 [DOI: https://doi.org/10.5185/amlett.2012.12482].

[34] Bhattacharyya, A., Chen, S. and Zhu, M., 2014. Graphene reinforced ultra-high molecular weight polyethylene with improved tensile strength and creep resistance properties. *Express Polymer Letters*, *8*(2) [DOI:10.3144/expresspolymlett.2014.10].

[35] Siddika, A., Al Mamun, M.A., Alyousef, R. and Amran, Y.M., 2019. Strengthening of reinforced concrete beams by using fiber-reinforced polymer composites: A review. *Journal of Building Engineering*, *25*, p.100798 [DOI: https://doi.org/10.1016/j.jobe.2019.100798].

[36] Gavande, V., Nagappan, S., Seo, B., Cho, Y.S. and Lee, W.K., 2023. Transparent nylon 6 nanofibers-reinforced epoxy matrix composites with superior mechanical and thermal properties. *Polymer Testing*, *122*, p.108002.

[DOI: https://doi.org/10.1016/j.polymertesting.2023.108002].

[37] Al-Zu'bi, M., Fan, M. and Anguilano, L., 2023. Parametric investigation of flexural performance of concrete prisms retrofitted with near-surface mounted FRP bars. *Composites Part C: Open Access*, p.100421 [DOI: https://doi.org/10.1016/j.jcomc.2023.100421].

[38] Iwahori, Y., Ishiwata, S., Sumizawa, T. and Ishikawa, T., 2005. Mechanical properties improvements in two-phase and three-phase composites using carbon nano-fiber dispersed resin. *Composites Part A: Applied Science and Manufacturing*, *36*(10), pp.1430-1439 [DOI: https://doi.org/10.1016/j.compositesa.2004.11.017].

[39] Zhou, Y., Pervin, F. and Jeelani, S., 2007. Effect vapor grown carbon nanofiber on thermal and mechanical properties of epoxy. *Journal of Materials Science*, *42*(17), pp.7544-7553 [DOI: 10.1007/s10853-007-1618-6].

[40] Al-Safy, R., Al-Mahaidi, R. and Simon, G.P., 2011. Thermal and mechanical characterizations of nanomaterial-modified adhesive used in bonding CFRP to concrete. *The Journal of Adhesion*, *87*(7-8), pp.842-857

[DOI: https://doi.org/10.1080/00218464.2011.597321].

[41] Zhu, J., Wei, S., Ryu, J., Budhathoki, M., Liang, G. and Guo, Z., 2010. In situ stabilized carbon nanofiber (CNF) reinforced epoxy nanocomposites. *Journal of Materials Chemistry*, *20*(23), pp.4937-4948 [DOI: https://doi.org/10.1039/C0JM00063A].

[42] Ladani, R.B., Wu, S., Kinloch, A.J., Ghorbani, K., Zhang, J., Mouritz, A.P. and Wang, C.H., 2016. Multifunctional properties of epoxy nanocomposites reinforced by aligned nanoscale carbon. *Materials & Design*, *94*, pp.554-564

[DOI: https://doi.org/10.1016/j.matdes.2016.01.052].

[43] Baruah, P. and Karak, N., 2016. Bio-based tough hyperbranched epoxy/graphene oxide nanocomposite with enhanced biodegradability attribute. *Polymer Degradation and Stability*, *129*, pp.26-33 [DOI: https://doi.org/10.1016/j.polymdegradstab.2016.03.021].

[44] Bao, C., Guo, Y., Song, L., Kan, Y., Qian, X. and Hu, Y., 2011. In situ preparation of functionalized graphene oxide/epoxy nanocomposites with effective reinforcements. *Journal of Materials Chemistry*, *21*(35), pp.13290-13298 [DOI: https://doi.org/10.1039/C1JM11434D].

[45] TK, B.S., Nair, A.B., Abraham, B.T., Beegum, P.S. and Thachil, E.T., 2014. Microwave exfoliated reduced graphene oxide epoxy nanocomposites for high performance applications. *Polymer*, *55*(16), pp.3614-3627 [DOI: https://doi.org/10.1016/j.polymer.2014.05.032].

[46] Kumar, A., Chouhan, D.K., Alegaonkar, P.S. and Patro, T.U., 2016. Graphene-like nanocarbon: An effective nanofiller for improving the mechanical and thermal properties of polymer at low weight fractions. *Composites Science and Technology*, *127*, pp.79-87 [DOI: https://doi.org/10.1016/j.compscitech.2016.02.028].

[47] Chandrasekaran, S., Seidel, C. and Schulte, K., 2013. Preparation and characterization of graphite nano-platelet (GNP)/epoxy nano-composite: Mechanical, electrical and thermal properties. *European Polymer Journal*, *49*(12), pp.3878-3888

[DOI: https://doi.org/10.1016/j.eurpolymj.2013.10.008].

[48] Park, S. and Kim, D.S., 2016. Curing behavior and physical properties of an epoxy nanocomposite with amine-functionalized graphene nanoplatelets. *Composite Interfaces*, *23*(7), pp.675-687 [DOI: https://doi.org/10.1080/09276440.2016.1168632].

[49] Chen, L., Zhao, P., Xie, H. and Yu, W., 2016. Thermal properties of epoxy resin based thermal interfacial materials by filling Ag nanoparticle-decorated graphene nanosheets. *Composites Science and Technology*, *125*, pp.17-21

[DOI: https://doi.org/10.1016/j.compscitech.2016.01.011].

[50] Thompson, L., Nikzad, M., Sbarski, I. and Yu, A., 2022. Esterified cellulose nanocrystals for reinforced epoxy nanocomposites. *Progress in Natural Science: Materials International* [DOI: https://doi.org/10.1016/j.pnsc.2022.05.001].

[51] Abraham, E., Kam, D., Nevo, Y., Slattegard, R., Rivkin, A., Lapidot, S. and Shoseyov, O., 2016. Highly modified cellulose nanocrystals and formation of epoxy-nanocrystalline cellulose

(CNC) nanocomposites. *ACS applied materials & interfaces*, *8*(41), pp.28086-28095 [DOI: https://doi.org/10.1021/acsami.6b09852].

[52] Aziz, T., Fan, H., Zhang, X., Khan, F.U., Fahad, S. and Ullah, A., 2020. Adhesive properties of bio-based epoxy resin reinforced by cellulose nanocrystal additives. *Journal of Polymer Engineering*, *40*(4), pp.314-320.

[53] Peng, S.X., Shrestha, S., Yoo, Y. and Youngblood, J.P., 2017. Enhanced dispersion and properties of a two-component epoxy nanocomposite using surface modified cellulose nanocrystals. *Polymer*, *112*, pp.359-368 [DOI: https://doi.org/10.1016/j.polymer.2017.02.016].

[54] Tanvir, A., El-Gawady, Y.H. and Al-Maadeed, M., 2017. Cellulose nanofibers to assist the release of healing agents in epoxy coatings. *Progress in Organic Coatings*, *112*, pp.127-132 [DOI: https://doi.org/10.1016/j.porgcoat.2017.07.008].

[55] Yue, L., Maiorana, A., Khelifa, F., Patel, A., Raquez, J.M., Bonnaud, L., Gross, R., Dubois, P. and Manas-Zloczower, I., 2018. Surface-modified cellulose nanocrystals for biobased epoxy nanocomposites. *Polymer*, *134*, pp.155-162

[DOI: https://doi.org/10.1016/j.polymer.2017.11.051].

[56] Johnsen, B.B., Kinloch, A.J., Mohammed, R.D., Taylor, A.C. and Sprenger, S., 2007. Toughening mechanisms of nanoparticle-modified epoxy polymers. *Polymer*, *48*(2), pp.530-541 [DOI: https://doi.org/10.1016/j.polymer.2006.11.038].

[57] Liu, Y.L., Wei, W.L., Hsu, K.Y. and Ho, W.H., 2004. Thermal stability of epoxy-silica hybrid materials by thermogravimetric analysis. *Thermochimica Acta*, *412*(1-2), pp.139-147 [DOI: https://doi.org/10.1016/j.tca.2003.09.004].

[58] Chisholm, N., Mahfuz, H., Rangari, V.K., Ashfaq, A. and Jeelani, S., 2005. Fabrication and mechanical characterization of carbon/SiC-epoxy nanocomposites. *Composite structures*, *67*(1), pp.115-124 [DOI: https://doi.org/10.1016/j.compstruct.2004.01.010].

[59] Morshed, S.A., Young, T.J., Chirdon, W.M., Zhang, Q. and Tatar, J., 2018. Durability of wet lay-up FRP bonded to concrete with nanomodified epoxy adhesives. *The Journal of Adhesion* [DOI: https://doi.org/10.1080/00218464.2018.1556647].

[60] Hosur, M., Mahdi, T.H., Islam, M.E. and Jeelani, S., 2017. Mechanical and viscoelastic properties of epoxy nanocomposites reinforced with carbon nanotubes, nanoclay, and binary

nanoparticles. *Journal of Reinforced Plastics and Composites*, *36*(9), pp.667-684 [DOI: https://doi.org/10.1177/0731684417691365].

[61] Huttunen-Saarivirta, E., Vaganov, G.V., Yudin, V.E. and Vuorinen, J., 2013. Characterization and corrosion protection properties of epoxy powder coatings containing nanoclays. *Progress in Organic Coatings*, *76*(4), pp.757-767

[DOI: https://doi.org/10.1016/j.porgcoat.2013.01.005].

[62] Al-Zu'bi, M., Anguilano, L. and Fan, M., 2023. Effect of incorporating carbon-and silicon-based nanomaterials on the physico-chemical properties of a structural epoxy adhesive. *Polymer Testing*, *128*, p.108221 [DOI: https://doi.org/10.1016/j.polymertesting.2023.108221].

Highlights

- NMEAs were considered for enhanced NSM-FRP flexural retrofitting systems.
- Using the silica, clay and graphite NMEAs increased capacities over the NE retrofits.
- CNF and cellulose NMEAs had a detrimental effect on the load capacities.
- The specimens' capacities decreased as the nanoparticles' wt.% increased.
- Using the carbon-based NMEAs could prevent the interfacial debonding.

The conflict of interest statement

☒ The authors declare that they have no known competing financial interests or personal relationships that could have appeared to influence the work reported in this paper.

☐The authors declare the following financial interests/personal relationships which may be considered as potential competing interests: